



University of  
**BRISTOL**

**School of Chemistry**

**The Use of Diamond Patterning Techniques in Pursuit  
of Controlling Cell Growth**

**Zoë Mills**

**This thesis is submitted in partial fulfilment of the requirements for the Honours Degree of BSc at  
the University of Bristol**

**Supervisor - Professor Paul May**

**Second Assessor - Dr Neil Fox**

**April 2016**

## **Acknowledgements**

First and foremost I would like to thank Dr Paul Nistor and Professor Paul May for their invaluable support and guidance throughout this project.

I would like to extend my appreciation to the rest of the Diamond Group who were on hand to answer any questions and queries that arose during this project.

Finally, thank you to my friends, family and partner for their continuous encouragement over the past year.

## **Abstract**

This thesis details an investigation into developing a technique for the patterning of diamond. In separate experiments, gold and copper tracks of 100  $\mu\text{m}$  width were evaporated onto silicon *via* the use of masks. Diamond was deposited onto these samples by chemical vapour deposition which was followed by washing the samples with an Aqua Regia solution. The surface of these samples were then analysed by scanning electron microscopy.

No disruption of the diamond surface grown over gold tracks was observed suggesting diamond is unable to be patterned in this manner. Diamond growth was found to be disrupted on areas of copper, and this disturbance was enhanced by treatment with Aqua Regia. However, this was ultimately unsuccessful in patterning the diamond.

## Contents Page

Acknowledgements .....	1
Abstract .....	2
<b>1 - Introduction - Diamond as a Substrate for Cells</b>	
▪ <b>1.1 - Properties of Diamond</b> .....	5
▪ <b>1.2 - Synthesis of Diamond</b> .....	6
▪ <b>1.2.1 - High Pressure, High Temperature</b> .....	6
▪ <b>1.2.2 - Chemical Vapour Deposition</b> .....	6
▪ <b>1.3 - Suitability of Diamond for Cell Growth</b> .....	9
▪ <b>1.3.1 - Biocompatibility</b> .....	9
▪ <b>1.3.2 - Surface Terminations</b> .....	9
▪ <b>1.3.3 - Boron Doping</b> .....	9
▪ <b>1.4 - Cells Grown on Diamond</b> .....	10
▪ <b>1.4.1 - Fibroblasts</b> .....	10
▪ <b>1.4.2 - Neuroblastomas</b> .....	11
▪ <b>1.4.3 - Pancreatic Carcinomas</b> .....	12
▪ <b>1.4.4 - Epithelial</b> .....	13
▪ <b>1.4.4.1 - Porcine Renal Epithelial</b> .....	13
▪ <b>1.4.4.2 - Human Epithelial</b> .....	13
▪ <b>1.4.5 - Vascular Endothelial</b> .....	14
▪ <b>1.4.6 - Osteoblasts</b> .....	15
▪ <b>1.4.7 - Stem Cells</b> .....	18
▪ <b>1.4.7.1 - Mesenchymal Stem Cells</b> .....	18
▪ <b>1.4.7.2 - Human Dental Stem Cells</b> .....	19
▪ <b>1.4.7.3 - Neural Stem Cells</b> .....	19
▪ <b>1.4.7.4 - Pluripotent Stem Cells</b> .....	20
▪ <b>1.5 - Cell Growth for Application within Implantable Diamond Electrodes</b> .....	21
▪ <b>1.5.1 - Electrode Activity</b> .....	21
▪ <b>1.5.1.1 - Amine Functionalised Surface</b> .....	21
▪ <b>1.5.2 - Electrode Capacitance</b> .....	22
▪ <b>1.5.2.1 - Surface Structuring <i>via</i> Carbon Nanotubes</b> .....	23
▪ <b>1.5.3 - Guided Cell Growth</b> .....	24
▪ <b>1.5.3.1 - Spatially Controlling Cell Growth</b> .....	24
▪ <b>1.5.3.1.1 - Spatial Control <i>via</i> Inkjet Printing</b> .....	24
▪ <b>1.5.3.1.2 - Spatial Control <i>via</i> Laser Etching</b> .....	25
▪ <b>1.5.3.2 - Diamond Coated Silicon Pillars</b> .....	25
▪ <b>1.5.4 - Future Prospects</b> .....	27
▪ <b>1.5.4.1 - BrainGate Project</b> .....	27
▪ <b>1.5.4.2 - Retinal Prosthetics</b> .....	27

<b>2 - Experimental - Developing Diamond Patterning Techniques</b>	
▪ <b>2.1 - Aims and Objectives</b> .....	29
▪ <b>2.2 - Methods and Materials</b> .....	30
▪ <b>2.2.1 - Gold (Sample A)</b> .....	30
▪ <b>2.2.2 - Copper</b> .....	31
▪ <b>2.2.2.1 - Copper Tracks on Silicon, Aqua Regia (Sample B)</b> .....	31
▪ <b>2.2.2.2 - Copper Tracks on Silicon, No Aqua Regia (Sample C)</b> .....	31
▪ <b>2.2.2.3 - Copper Layer on Silicon, No Aqua Regia (Sample D)</b> .....	31
▪ <b>2.2.2.4 - Copper Layer on Silicon, No CVD (Sample E)</b> .....	31
▪ <b>2.3 - Results and Discussion</b> .....	32
▪ <b>2.3.1 - Gold</b> .....	32
▪ <b>2.3.2 - Copper</b> .....	32
▪ <b>2.4 - Conclusion</b> .....	38
<b>3 - References</b> .....	40

# 1 - Introduction - Diamond as a Substrate for Cells

## 1.1 - Properties of Diamond

Diamond is an allotrope of carbon, with all the atoms arranged in a covalently bonded,  $sp^3$  hybridised tetrahedral lattice. Another allotrope of carbon, and the most stable one, is graphite. Graphite has a planar arrangement of  $sp^2$  carbon sheets. The reason for the existence of diamond, and not just graphite, is due to the very large energy barrier required for the inter-conversion of diamond to graphite. This activation barrier is large because there is no simple mechanism for the conversion, and thus the energy is comparable to destroying the covalently bonded diamond lattice. This causes diamond to be a metastable form. The relationship between diamond and graphite can be visualised through a carbon phase diagram, shown in Figure 1.1.<sup>1</sup>

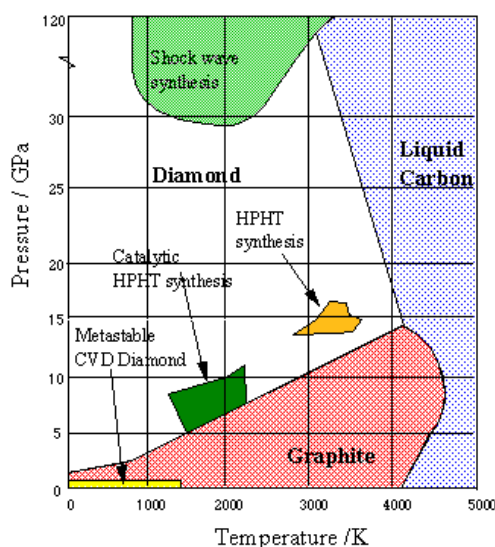


**Figure 1.1:** Phase diagram for carbon.<sup>1</sup>

Apart from being an attractive, and highly sought-after, gemstone; diamond is renowned within the scientific community for its extraordinary physical properties. As a direct result of the covalent lattice, diamond is the hardest natural material known. Some other important properties of diamond are summarised below, in Table 1.1.

Hardness	10000 kg mm <sup>-2</sup>
Tensile strength	>1.2 GPa
Compressive strength	>110 GPa
Young's modulus	1220 GPa
Density	3.52 g cm <sup>-3</sup>
Thermal expansion coefficient	1.1x10 <sup>-6</sup> K <sup>-1</sup>
Thermal conductivity	20 W cm <sup>-1</sup> K <sup>-1</sup>
Resistivity	10 <sup>13</sup> – 10 <sup>16</sup> Ω cm

**Table 1.1:** The physical properties of diamond.<sup>2</sup>

In addition to the quantitative properties listed in Table 1.1, diamond is also chemically inert, biologically compatible and wear-resistant. Furthermore, by substituting some of the carbon atoms within the lattice with boron atoms, it is possible to alter the electrical conductivity of diamond as well. This is known as boron doping.

## **1.2 - Synthesis of Diamond**

All of the aforementioned properties of diamond have made the material the focus of many potential applications. However, investigations with diamond were initially limited due to the scarcity and expense of the material. This led to the need to develop a method to synthesise diamond.

### **1.2.1 - High Pressure, High Temperature**

Natural diamond is formed deep underground, where carbon is exposed to high temperatures and pressure. This knowledge led to the development of the high-pressure, high-temperature (HPHT) method of diamond growth. Although synthetic diamond has been produced through this technique for several decades, the method and diamond produced had significant limitations. The extreme conditions required during the HPHT process (over 2000 K and up to 100,000 atm) lead to undesirable high energy costs.<sup>3</sup> Furthermore, HPHT produces single crystal diamonds which are not gem-stone quality, and main applications are limited to cutting and polishing tools. These shortcomings resulted in a need to explore different, more efficient, ways to synthesise diamond and so chemical vapour deposition (CVD) was developed.

### **1.2.2 - Chemical Vapour Deposition**

Chemical vapour deposition was initially developed to reflect the idea that carbon atoms could be sequentially added to one another leading to the formation of a tetrahedral network, identical to the structure of diamond. The production of diamond film was initially investigated by Eversole and Deryagin, although issues arose from the decomposition of gases containing only carbon.<sup>4, 5</sup> Both investigations found that graphite was also being deposited onto the diamond substrate, thus leading to impure samples containing a mix of diamond and graphite.

This barrier was overcome by Angus *et al.* who discovered the vital addition of atomic hydrogen to the CVD process.<sup>6</sup> Hydrogen atoms were shown to etch graphite at a faster rate than diamond, meaning that graphite was removed back to the gas phase, leaving only pure diamond on the substrate. This led to further studies surrounding CVD, including the use of non-diamond substrates, and ultimately led to the formation of the first hot filament CVD reactor in 1982.<sup>7-9</sup>

In all CVD reactors, the process gases (typically methane diluted in hydrogen at approximately a 1-2% mixing ratio) must be activated first. This activation can occur through several different methods, including the use of a hot filament, microwave and an oxyacetylene torch (Figure 1.2.2a).<sup>10</sup>

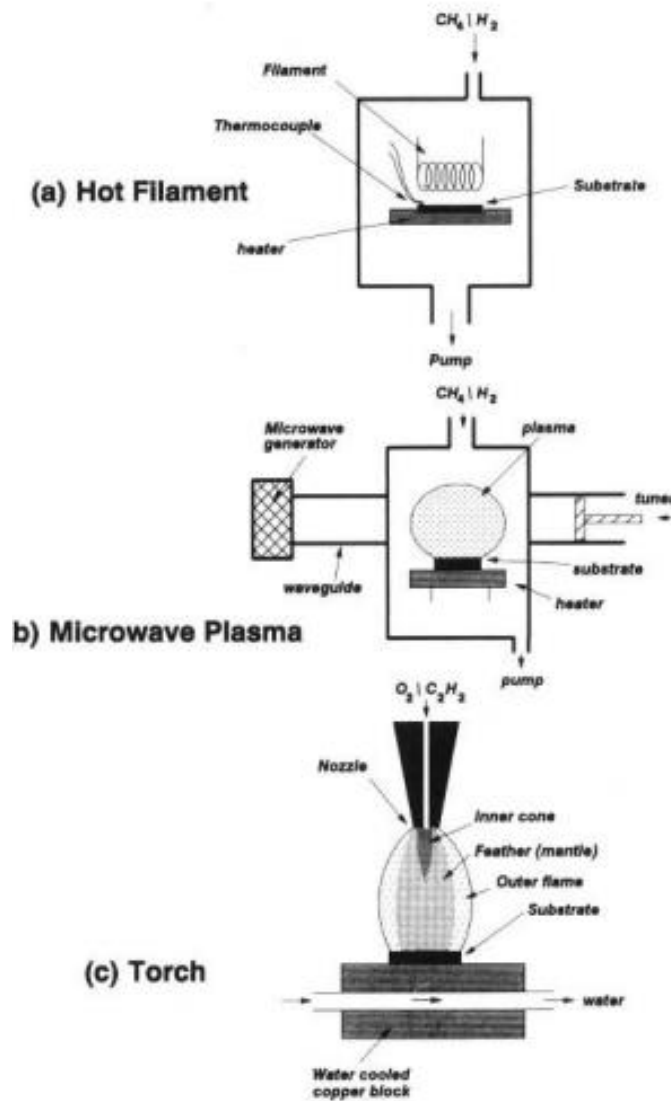


**Figure 1.2.2a:** Common types of low pressure CVD reactors. (a) Hot filament (b) Microwave plasma enhanced CVD reactor (c) Oxyacetylene torch.<sup>10</sup>

This activation process produces reactive atoms and radicals from the parent molecules, and also forms electrons and ions. Once past the activation region, these particles undergo several chemical processes before they finally come into contact with the substrate. Within the diffusion layer above the substrate, the species may transfer back into the gaseous phase or absorb to the surface at a suitable site. Once absorbed to the surface of the substrate, a chemical reaction may take place which forms diamond.<sup>11</sup> This process is illustrated in Figure 1.2.2b.

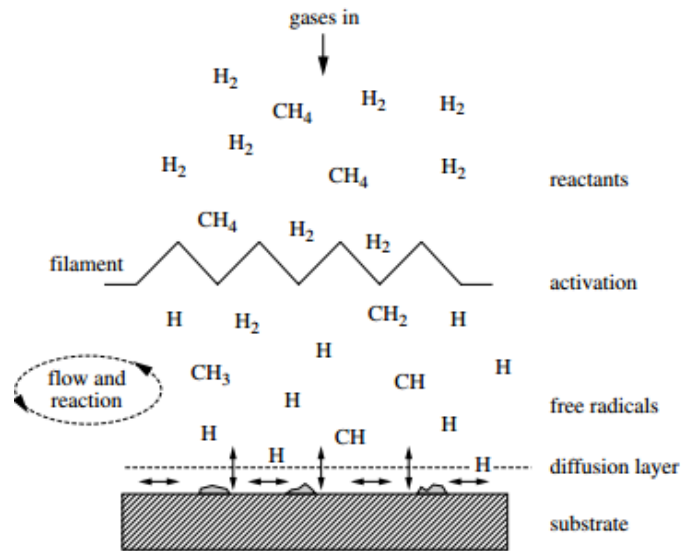


**Figure 1.2.2b:** Chemical and physical processes involved during diamond CVD.<sup>11</sup>

After many years of research, the Bachmann triangle diagram (Figure 1.2.2c) was developed.<sup>12</sup> This compiled the compositions of carbon, hydrogen and oxygen needed for diamond growth. The diagram was composed of research from over 70 deposition experiments, including using different gases and carrying out the experiments in different reactors. From this, Bachmann deduced that the single factor that dictated diamond growth was the requirement of the composition of gases to be close to or above the CO line, as opposed to other factors, such as the CVD system or gas mixtures.

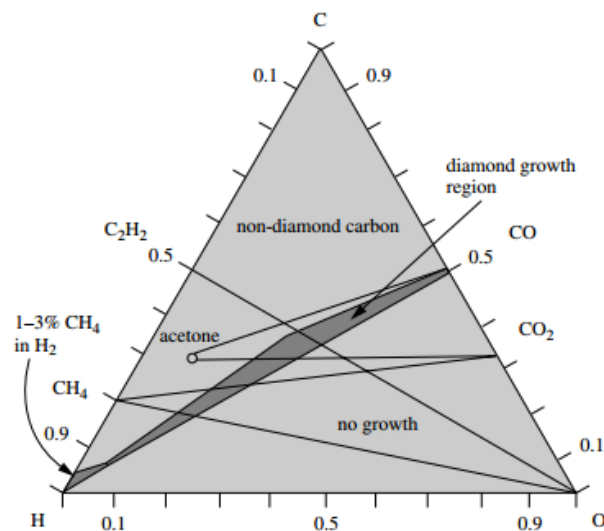


**Figure 1.2.2c:** Simplified Bachmann triangle C-H-O composition diagram. Below the CO line, no film growth is observed. Above CO line, non-diamond carbon deposited, except in window close to line, which forms polycrystalline diamond films. Most experiments involving few per cent CH<sub>4</sub> in H<sub>2</sub> are constrained to small region in left hand corner.<sup>11</sup>

Synthesizing CVD diamond through a gas phase, thus reducing expenses in comparison to the extreme conditions of the HPHT method, combined with the ability to extend applications of diamond through the production of diamond film, has meant that CVD diamond has become a well-researched area.

### 1.3 - Suitability of Diamond for Cell Growth

The production of nanocrystalline diamond (NCD) films through CVD has facilitated research into many areas. As seen earlier, diamond is hard, wear-resistant and chemically inert. These properties are ideal for use as an implantable material as they provide biocompatibility and the ability to withstand the enzymatic conditions within the body. This has great appeal within the medical field, in particular the development and application of diamond coated implants ranging from structural orthopaedic implants to electrode-like implants for combatting nerve and spinal injuries.

#### 1.3.1 - Biocompatibility

Implantable diamond is a possibility due to the reduced immune response the body shows on contact with diamond. This is observed through both *in vivo* and *in vitro* studies which have shown that NCD produces minimal toxic effect on biological systems.<sup>13, 14</sup>

Another important criterion for implantable material is the level of bacterial resistance. On comparison with other known implant materials, namely titanium and medical-grade steel, it was found that NCD was most resistant to bacterial infection, shown through measurement of *E. coli* colonisation.<sup>15</sup>

#### 1.3.2 - Surface Terminations

An important factor to the success of diamond implants is the ability to grow cells on its surface. NCD made by CVD has a surface naturally terminated with hydrogen. There exist multiple pathways to changing these surface terminations to, most commonly, oxygen and nitrogen based moieties. Some common ways to create these surface terminations include treatment with oxygen plasmas and acid chemistry.<sup>16, 17</sup> This changes the polarity of the surface and can potentially enhance the possibility of cell growth by increasing initial cell adhesion to the surface. The surface polarity is related to its hydrophilicity.

*In vivo* cell adhesion is mediated through an extracellular matrix (ECM), which is the term for molecules that surround the cell that provide structure as well as biochemical support. However, an ECM does not exist during cell adhesion to an artificial substrate. *In vitro* studies can rely on adhesion proteins to mimic a basic ECM and so specific proteins such as fibronectin, vitronectin and laminin greatly facilitate the adhesion of cells. Increasing the hydrophilicity of the diamond surface, through addition of -OH, -COOH and -NH<sub>2</sub> surface terminations, has the effect of promoting adsorption of these specific proteins; which in turn increases cell adhesion.<sup>18</sup>

#### 1.3.3 - Boron Doping

The actual growth of cells on its surface is not the only obstacle towards successful implantation of diamond. Cells like neurons are dependent on electrical activity and therefore the diamond surface must be able to support this. By way of boron doping, it is possible to increase the electrical conductivity of diamond so much that it becomes a *p*-type semiconductor.<sup>19</sup> The band gap for diamond is ~5.5 eV, the reason for its insulating properties.<sup>20</sup> The inclusion of boron which, due to having less valence electrons than carbon, is an acceptor creates a band structure with an activation energy of only ~0.39 eV, as seen in Figure 1.3.3.<sup>20</sup>

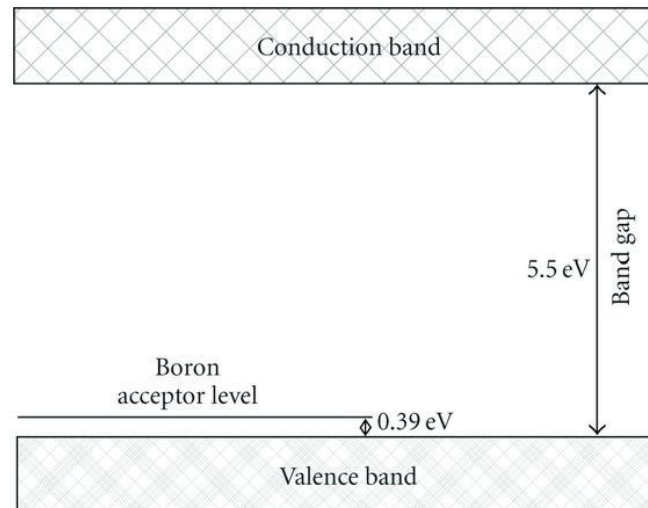


**Figure 1.3.3:** Band gap structure for diamond with the boron acceptor level shown.<sup>20</sup>

Boron doping is consequently essential for certain cell cultures. Boron-doped diamond (BDD) substrates can be created by manipulating the CVD process. The use of diborane gas ( $B_2H_6$ ) is prevalent in this matter despite the toxicity, and it has been shown the B-doped diamond product is not, itself, toxic.<sup>21</sup>

The promising future of implantable diamond is supported by research into how exactly the diamond substrate can be altered and how this affects the adhesion, growth and viability (capability of life) of all types of cells. This research has vastly increased, and the range of cells successfully grown on diamond has risen.

## 1.4 - Cells Grown on Diamond

### 1.4.1 - Fibroblasts

Fibroblasts, the cells that produce collagen, are a readily accessible cell source. This has made them a good candidate for testing the growth of cells on a diamond substrate. Chong *et al.* have shown that fibroblasts undergo pronounced growth on a diamond surface with smaller crystals and a polarized surface, resulting from oxygen termination.<sup>22</sup> The impact of the difference in crystal size of ultrananocrystalline diamond (UNCD) and microcrystalline diamond ( $\mu$ CD) was investigated, alongside the influence of oxygen terminating the surface. The oxygen functionalization of the surface was arrived at via treatment with undecylenic acid or UV radiation and the difference in effects was recorded.

Through atomic force microscopy (AFM), the adhesion forces for initial cell-surface interaction was recorded for functionalized and non-functionalized  $\mu$ CD and UNCD. On comparison, UNCD required a larger maximum de-adhesion force than  $\mu$ CD.

On both  $\mu$ CD and UNCD the de-adhesion forces were further increased after functionalization of the surface. Treatment with UV light led to the greatest increase in de-adhesion forces on both surfaces, suggesting that this method of functionalization is superior to the use of undecylenic acid. Cell-surface interaction for UNCD treated with UV light was observed to form an average of seven bonds

during adhesion whilst hydrogen terminated diamond recorded the average formation of two bonds.

The subsequent cell growth was also measured, finding that cell density was also highest on UNCD treated with UV light. Although functionalization of the diamond surface observed a substantial increase in cell viability on the  $\mu$ CD, UNCD was recorded to have a greater cell growth of fibroblasts on all surfaces. Human dermal fibroblasts that have grown on oxygen terminated (O-) surfaces are shown, in Figure 1.4.1, to exhibit spindle-like morphology similar to the fibronectin-coated control. The unaltered hydrogen terminated (H-) surface showed round morphology, suggesting cells have not adhered correctly due to the hydrophobic surface.

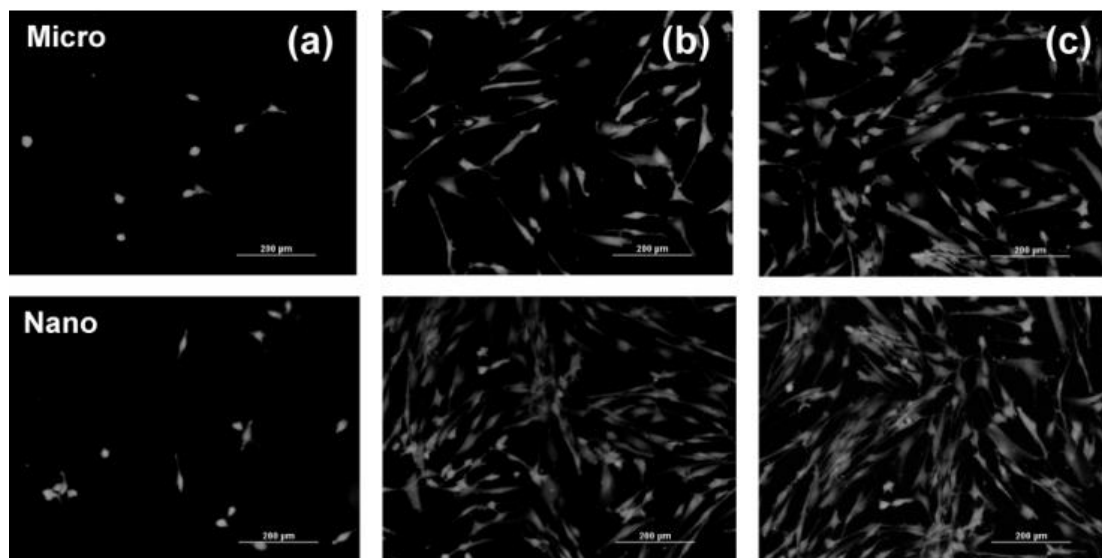


**Figure 1.4.1:** Fluorescence micrographs showing normal human dermal fibroblast cells on (a) H-terminated (b) Undecylenic acid functionalised (c) UV treatment diamond surfaces.<sup>22</sup>

The small grain size of UNCD leads to an increase in surface area, meaning there is a greater area for cell membranes to interact with. This ultimately leads to an increase in cell adhesion, as more bonds are formed with the surface. By functionalizing the surface with acid or UV light, the surface was altered to become hydrophilic which caused an increase in initial cell adhesion.

#### 1.4.2 - Neuroblastomas

Whilst investigating modifications to nanocrystalline diamond coatings, Vaitkuviene *et al.* grew the cancerous neuroblastoma SH-SY5Y cell line to ensure the biocompatibility of the diamond coating.<sup>23</sup> Prepared via microwave plasma chemical vapour deposition (MPCVD), the NCD coating was subjected to alterations by way of H- and O-surface termination and boron doping. This investigation into growing the neuroblastomas took place with and without the addition of the cell medium fetal bovine serum (FBS). FBS is a common supplement for cell cultures as it contains many growth factors. The SH-SY5Y cell line directly placed onto the altered NCD coatings showed that adhesion and proliferation took place on all surfaces, regardless of the addition of FBS. Light microscopy was used to monitor cell adhesion, proliferation and morphology. It was found the cells maintained a similar morphology on all surfaces.

The report found that after 48 hours of cultivation, cell proliferation was greatest in samples containing FBS. Under these favourable conditions, SH-SY5Y was found to produce elastin microfibril interface located protein (EMILIN-1). This extracellular glycoprotein is known to increase cell adhesion.

On comparison, samples containing no medium were found to have a more diverse expression of proteins and EMILIN-1 was not produced at all. Furthermore, the appearance of heat shock proteins (HSP) was noted. This suggests that due to the lack of FBS, unfavourable conditions caused the cells to undergo extensive stress, culminating in the production of HSPs instead of EMILIN-1, thus reducing cell adhesion.

When compared to the control (fused silica), the H- and O-terminated surfaces of diamond were shown to be far more proficient at the adhesion and proliferation of neuroblastoma cells, with increased proliferation rates of 20 and 58% in FBS and FBS-free mediums respectively. This proficiency was further increased by increasing the dopant level of boron from 0 to 10000 ppm.

### **1.4.3 - Pancreatic Carcinomas**

Neuroblastomas are not the only cancerous cells to have been grown on NCD surfaces. Klauser *et al.* used a human pancreatic carcinoma (PANC-1) cell line to display the difference in FBS-mediated and direct cell adherence to NCD surfaces with varying degrees of wettability.<sup>24</sup> The wettability of the NCD surfaces was controlled through differing surface terminations. Four surface chemistries were prepared: a hydrophobic H-terminated surface (H-NCD), a hydrophobic F-terminated surface (F-NCD, via fluorine plasma), a hydrophilic O-terminated surface (O-NCD, via sulfochromic acid) and a hydrophilic partially O-terminated surface (pO-NCD, via thermal treatment in air). The topologies and roughness of these surfaces was kept constant throughout.

It was found that cell adhesion on the hydrophilic surfaces was independent of the addition of the FBS serum. The clean, hydrophilic O-NCD and pO-NCD surfaces are able to support direct cell adhesion, and in the FBS containing serum the hydrophilicity of these surfaces is actually reduced. This is due to the adsorption of amphiphilic proteins in the FBS serum, as they increase the proportion of hydrophobic groups pointing away from the surface. For the hydrophobic (H-NCD and F-NCD) surfaces, cell adhesion was found to be impossible without the addition of FBS. When immersed in the FBS containing serum, it was found that cell adhesion did occur, although at a lower rate than for the hydrophilic surfaces. The adhesion of cells to the hydrophobic surface must, therefore, be mediated through the amphiphilic proteins. These results can be observed directly in Figure 1.4.3.

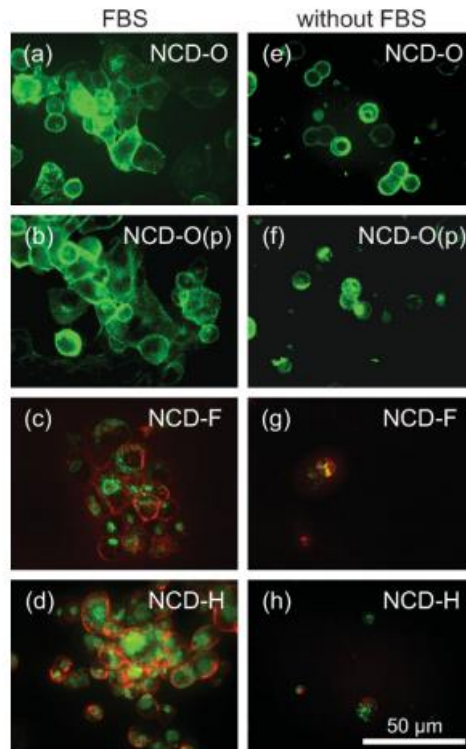


**Figure 1.4.3:** Human pancreatic carcinoma cells grown on differently terminated NCD surfaces in a FBS ((a) to (d)) and FBS-free ((e) to (h)) medium. Images of cells grown on O-NCD and pO-NCD surfaces were taken after 24 hours, with freshly added wheat germ agglutinin (WGA), that is bound to the cell surface, displayed in green. Images of cells grown on F-NCD and H-NCD surfaces were taken after 72 hours, with freshly added WGA displayed in red and internalized WGA shown in green.<sup>24</sup>

#### 1.4.4 Epithelial

##### 1.4.4.1 Porcine Renal Epithelial

In the above report by Klauser *et al.*, porcine renal epithelial cells (LLC-PK1) were grown on the same surfaces under identical conditions.<sup>24</sup> Cell adhesion was observed to be affected in the same way as for the PANC-1 cells but in a much more pronounced manner, as can be seen in Figure 1.4.4.1, where cell adhesion to the hydrophilic surfaces in the FBS-free medium is much more obvious.

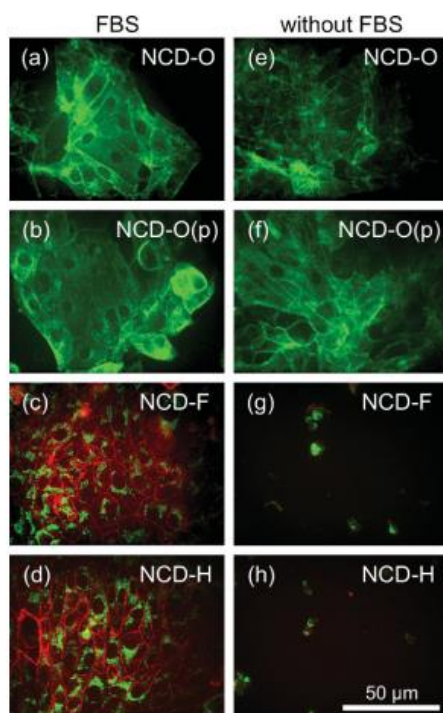


**Figure 1.4.4.1:** Porcine renal epithelial cells grown on differently terminated NCD surfaces in a FBS ((a) to (d)) and FBS-free ((e) to (h)) medium. Images of cells grown on O-NCD and pO-NCD surfaces were taken after 24 hours, with freshly added wheat germ agglutinin (WGA), that is bound to the cell surface, displayed in green. Images of cells grown on F-NCD and H-NCD surfaces were taken after 72 hours, with freshly added WGA displayed in red and internalized WGA shown in green.<sup>24</sup>

#### 1.4.4.2 - Human Epithelial

In the growth of human epithelial cells on nanocrystalline diamond by Rezek *et al.*, two distinct cell morphologies were found depending on the NCD surface terminations.<sup>25</sup> For H-NCD, round cells were observed with barely visible cytoplasmic rims (edges of the cell), as seen in Figure 1.4.4.2. In the O-NCD substrate the cells were elongated and had significantly more enhanced cytoplasmic rims, and their nucleoli were also visible. Cells were better adhered to the O-NCD substrate than H-NCD, which can be explained by the change in conformation of the protein layer adsorbed onto the diamond surface from the medium. The O-terminations provide more favourable protein morphologies for the adhesion of epithelial cells. However, both NCD systems had increased adherence in comparison to a glass standard, suggesting that the medium proteins do not adhere as strongly to glass as to NCD.

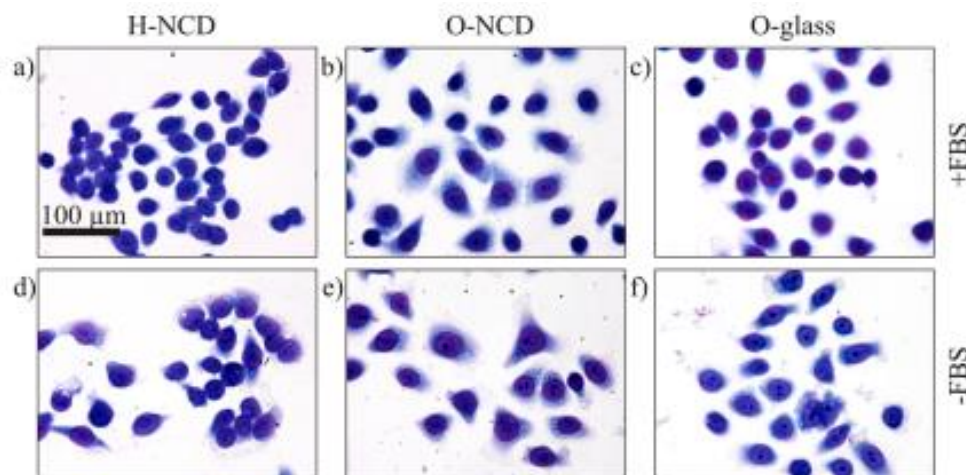


**Figure 1.4.4.2:** Optical microscope fluorescence images of stained epithelial-type cells grown on differently terminated nanocrystalline diamond and a glass reference, with and without FBS.<sup>25</sup>

#### 1.4.5 - Vascular Endothelial

Further cell types that have shown a response to modification of the NCD surface have been reported. Grausova *et al.* experimented with the surface roughness of NCD films in the adhesion, growth and viability of bovine pulmonary artery endothelial (CPAE) cells.<sup>26</sup> NCD diamond films with RMS values of 8.2 nm and 301 nm were prepared by nanostructuring and hierarchically micro-nanostructuring (microstructured surfaces patterned with nanoscale features) respectively. These substrates were compared with plain silicon substrates of similar roughness, RMS values of 1 nm and 300 nm.

Throughout the five day cultivation period it was found that cell adhesion was significantly higher on both NCD films in comparison to the plain Si substrates. Viability of the adhered cell populations were high on both the NCD films, ranging from 96% to 100%. Although there were markedly reduced cell populations on Si, the viability of these cells still remained high.

It was found that endothelial cell growth was sensitive to surface roughness, as a much higher cell density was observed on the purely nanostructured NCD film than the micro-nano NCD film after three days. This may be explained by the CPAE growth being obstructed by the micro-sized surface topology.<sup>27</sup> Despite this, over the entire five day period both NCD substrates allowed for growth of similar size populations. These observations lead to the conclusion that NCD films may be suitable substrates for tissue engineering applications involving endothelial cells.

#### 1.4.6 - Osteoblasts

In a similar manner to endothelial cells, tissue engineering can be applied to osteoblasts (cells which produce bone) and could offer a promising future for the improvement of artificial orthopaedic implants. Current titanium orthopaedic implants experience corrosion and immune responses from the body which can lead to the non-ideal situation of replacing the implant, especially amongst those with diabetes and other health risks.<sup>28</sup> The known biocompatibility and resilience of diamond led to studies whereby titanium was coated in diamond *via* CVD in efforts to protect the base

titanium substrate. As expected this produced a reduction in the corrosion of the implant, however further study was needed to ensure that bone surrounding the implant carried on being produced.<sup>29</sup>

Osteoblasts have been shown to grow on NCD surfaces with varied surface roughness. Grausova *et al.* grew human osteoblast-like cells (MG 63 cell line) on NCD surfaces that were nanostructured and micro-nanostructured.<sup>26</sup> It was found that there was no difference in cell number when comparing the two NCD surfaces. The MG 63 cells were also grown on plain Si substrates with similar roughness and the viability of these cells was found to rapidly decrease over five days to the point where no MG 63 cells were found on the silicon. This suggests that these cells are susceptible to the cytotoxicity (toxicity to cells) of silicon.

Pareta *et al.* investigated the growth of osteoblasts on diamond coated titanium as a step further in combatting the issue of corrosion-resistant implants.<sup>30</sup> Throughout the MPCVD process to coat diamond onto titanium, the concentration of hydrogen was increased sequentially (to 2, 5, 10 and 15%) during film growth onto different titanium substrates.

It was found that the NCD coating that contained the highest concentration of hydrogen present in the film provided the greatest surface roughness, though all NCD surfaces provided rougher surfaces on comparison with uncoated titanium. However, this did not lead to the most successful adhesion and growth of cells. This is suggested to be due to the roughness of the surface is much higher ( $92.5 \pm 18.7$  nm) compared to natural bone (70 nm).<sup>31</sup> Furthermore, the higher concentrations of hydrogen also led to uneven and poor quality NCD coatings which could have also contributed to the lack of osteoblast adhesion.

The substrate containing 5% hydrogen in the film provided the most favourable conditions and thus exhibited the greatest osteoblast adhesion and spreading on the surface of diamond. This optimised substrate was further investigated by varying the surface chemistry via plasma treatments containing oxygen and ammonia, causing the surface to be terminated by  $-OH$  and  $C=O$ , and  $-NH_2$ , respectively. Both plasma treatments led to a significant rise in the density of cells formed on the surface of the diamond, and treatment with ammonia saw a further increase in cell density over the substrate treated with oxygen. This rise in cell density is as a result of the increased surface hydrophilicity, as explained in section 1.3.2.

Alteration of the surface functionalization through plasma treatment has also been reported by Yang *et al.*<sup>32</sup> By using substrates with known surface roughness and only changing the surface terminations, it was reported that osteoblast response to NCD was greatest after plasma treatment with ammonia (Figure 1.4.6a). The success of this osteoblast-NCD interface is again suggested to be due to the greater surface energy (attributed to the increase in polar components) exhibited from the surface treated with ammonia on comparison with the surfaces terminated with oxygen or hydrogen.

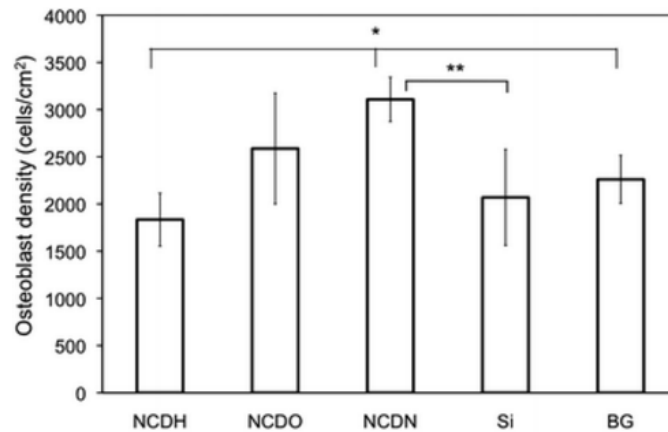


**Figure 1.4.6a:** Osteoblast attachment on hydrogen terminated NCD, oxygen terminated NCD, amino terminated NCD (NCDN) and Si and borosilicate glass (BG), both acting as controls, after 12 hours of culture. Osteoblast seeding density was  $10^4$  cells  $\text{cm}^{-2}$ . Data are expressed as the mean  $\pm$  standard deviation of the mean (N = 3). \* $p < 0.05$ , \*\* $p < 0.1$ .<sup>32</sup>

Fluorescence microscopy images (Figure 1.4.6b) showed both oxygen and amino terminations to exhibit the greatest number of cell-cell interactions along with thick individual filaments, suggesting increased interactions between the substrate and cell.

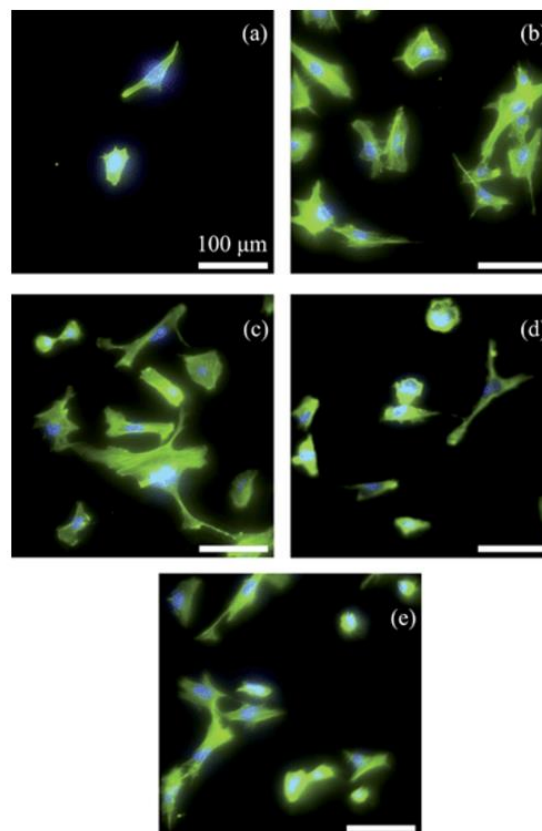


**Figure 1.4.6b:** Fluorescence microscopy images showing osteoblast morphology on H-NCD (a), O-NCD (b), NCDN (c), Si (d) and borosilicate glass (e) after 12 hours of culture (bar = 100  $\mu\text{m}$ ). Osteoblasts were stained by rhodamine phalloidin and the nuclei were stained by DAPI.<sup>32</sup>

## 1.4.7 - Stem Cells

### 1.4.7.1 - Mesenchymal Stem Cells

A more recent investigation into CVD diamond coatings for titanium alloys was conducted by Strąkowska *et al.* in relation to the effect of the electrochemical assisted deposition (ECAD) of a hydroxyapatite (HAp) top layer on growth of human mesenchymal stem cells (hMSCs) in an osteogenic differentiation medium.<sup>33</sup> Mesenchymal stem cells can differentiate into many types of cell; myocytes (muscle cells), adipocytes (fat cells), chondrocytes (cartilage cells) and osteoblasts, so the specific medium is important to ensure controlled differentiation.

The HAp coating was applied to a  $Ti_6Al_4V$  alloy and it was reported that cell proliferation was increased for this coating, although initial cell adhesion was greater in the case of a single boron-doped NCD (B-NCD) coating. The two-layer coating is expected to show an additive corrosion resistance, wear resistance and display favourable osteoconductivity (process whereby growth of bone on a surface occurs), which may be worth a small loss in adhesion. It was found that the HAp coating adhered better to a B-NCD substrate, than an undoped NCD substrate, due to the higher electrical conductivity.

Further work on the interaction of MSCs with diamond substrates was conducted by Clem *et al.*, who reported on the adhesion of MSCs to H-, O- and F- terminated ultra-smooth nanostructured diamond (USND) surface coatings.<sup>34</sup> A comparison of H-USND with bare  $Ti_6Al_4V$  alloy and cobalt chrome (CoCrMo) was also made.

It was found that for MSCs, cell adhesion was supported by the H-USND surface but resisted by the O-USND and F-USND surfaces. Images of MSC growth on these surfaces is shown below in Figure 1.4.7.1a.

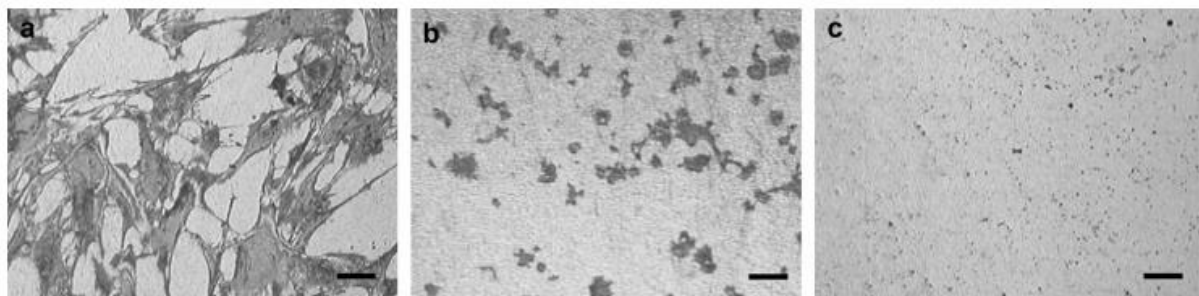


**Figure 1.4.7.1a:** Reflected light microscopy images showing cultures of MSCs on (a) hydrogen terminated USND, (b) oxygen terminated USND and (c) fluorine terminated USND.<sup>34</sup>

As the only viable candidate for the growth of MSCs, H-USND was used to compare cell behaviour with  $Ti_6Al_4V$  and CoCrMo. The adhesion of MSCs on H-USND was found to be greater than for CoCrMo, but less than on  $Ti_6Al_4V$ . However, the usefulness of  $Ti_6Al_4V$  is limited by its low hardness, hence the investigation into other materials. While the adhesion of MSCs is lower for H-USND than  $Ti_6Al_4V$ , viability assays showed that the viable cell populations on these surfaces were very similar. These results are displayed in Figure 1.4.7.1b.

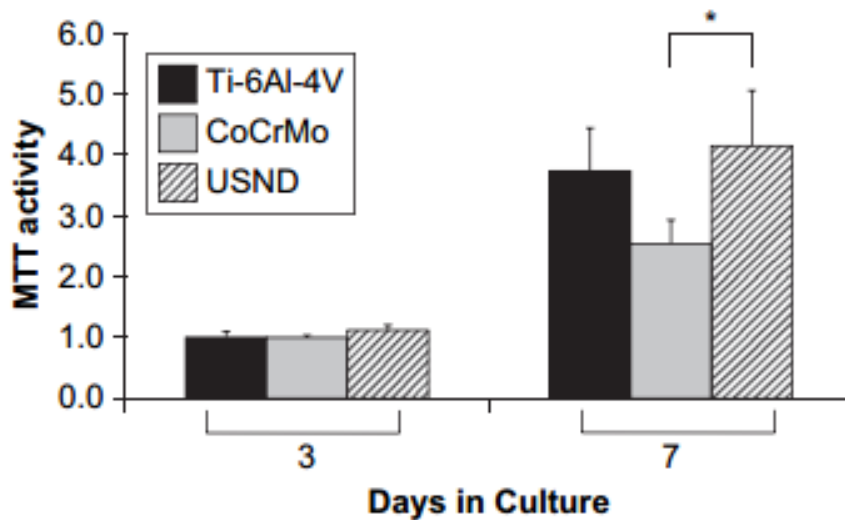


**Figure 1.4.7.1b:** MTT proliferation assays to show cell activity of MSCs after exposure to Ti<sub>6</sub>Al<sub>4</sub>V, CoCrMo and H-USND for up to one week.<sup>34</sup>

#### 1.4.7.2 - Human Dental Stem Cells

The ability to grow human dental stem cells (hDSCs) is of great interest in the field of tissue engineering, specifically tooth tissue engineering. Theoretically, growth of a culture of hDSCs on a biocompatible scaffold could lead to the possibility of whole tooth regeneration. Duailibi *et al.* investigated the use of NCD as a substrate in growing hDSCs, in particular the effect of H- and O-terminated surfaces on cell growth and mineral deposition.<sup>35</sup>

After characterisation by flow cytometry hDSCs were seeded onto NCD discs of alternative H- and O-terminated regions. Following a 28 day growth period it was found, through SEM and EDS analysis, that a much higher deposition of calcium, oxygen and phosphorus was observed on the O-terminated surface. It was concluded that a considerably more developed extracellular matrix was present on the O-terminated surface, indicating a higher probability of forming the enamel and dentin tissues required for tooth formation.

#### 1.4.7.3 - Neural Stem Cells

The effect of H- and O- terminated UNCD films on the proliferation and differentiation of neural stem cells (NSCs) has also been investigated. NSCs primarily differentiate into neurons, oligodendrocytes (cells that provide support and insulation to neurons) or astrocytes (glial cells, involved in the immune response), and therefore it is important to understand the factors involved in differentiation. Chen *et al.* cultured NSCs on polystyrene with a top coating of poly-D-lysine (PS), H-UNCD or O-UNCD.<sup>36</sup> It was found that cell proliferation was not significantly reduced on either UNCD surface compared to the PS standard. The main point of this investigation, however, was relevant to the differentiation observed for each NSC culture on the different surface types in the absence of any external growth factors. Promotion of NSC differentiation has previously been mediated through the use of specific differentiating mediums, but it was shown that these were not necessary for the UNCD surfaces. It was noted that upon comparison to the PS standard, the H-surface incited preferential differentiation to neurons, while the O- surface favours oligodendrocyte differentiation.

#### 1.4.7.4 - Pluripotent Stem Cells

An investigation by Nistor *et al.* compared the ability of human induced-pluripotent stem cells (hIPS) survival on differing diamond surfaces.<sup>37</sup> hIPS are formed from isolated adult cells that have been induced to become pluripotent. They also possess the ability to differentiate into any cell type.

The diamond surface roughness in this experiment varied from polished diamond, to polycrystalline diamond with a ranging crystallite size. By controlling the length of the CVD process, the size of the crystallites produced on silicon substrates could be varied and thus the surface roughness could be altered. All surfaces were found capable of cell growth and survival, though all microcrystalline diamond surfaces were seen to provide more favourable conditions than polished diamond. The hIPS cultures observed were found to have differentiated into a mixture of neurons and astrocytes.

The differentiation protocols reported includes the use of a bovine serum albumin, and the ultimate goal will be to preclude the use of such xeno-materials in order to simulate a truly human growth process. This can be achieved by either the usage of a human albumin, which is a limited resource, or by complete removal of any albumin which will lead to challenging conditions over the long culture period.

It was found that a shorter deposition time, producing smaller crystals, led to a denser concentration of neurons present during the immunofluorescence process. Polished diamond and substrates that had undergone the CVD process for longer than four hours were shown to have several areas where there were few or no neurites present. It was reported that the once the distance between the crystals exceeded 1  $\mu\text{m}$ , the efficiency of neurite (projection from the neuron cell body) production decreased considerably, as summarised in Figure 1.4.7.4.

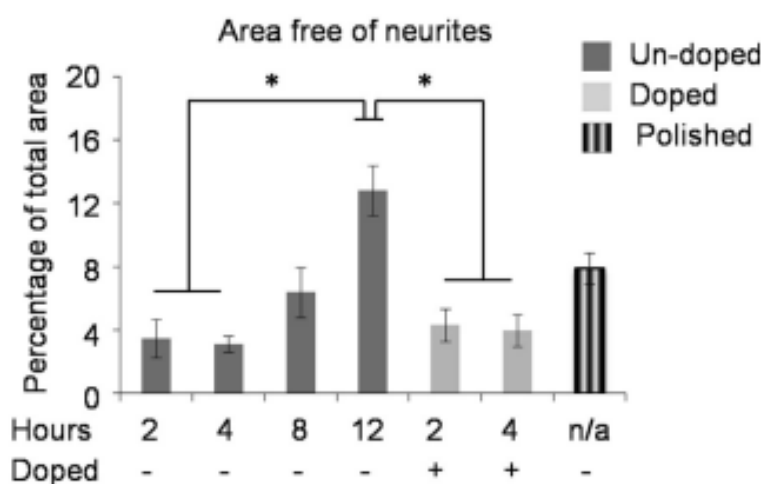


**Figure 1.4.7.4:** Bar graph showing the percentage of total surface area that is devoid of neurites for diamond substrates with differing crystal size. Crystal size was determined by the duration of the CVD process. Error bars are representative of the error of the mean,  $*p < 0.05$ .<sup>37</sup>

Boron doping is essential for the functioning of the neuron cultures, as mentioned earlier, and it was found that incorporating boron into the diamond had no adverse influence on either cell survival or neurite formation, regardless of the boron concentration used.

## 1.5 - Cell Growth for Application within Implantable Diamond Electrodes

The ability to grow human neural stem cells (hNSCs) and hIPS, and direct their differentiation into neurons, on diamond is of great interest for research and development surrounding implantable diamond electrodes; perhaps one of the most promising applications for diamond cell growth. An implantable electrode operates by either recording electrical impulses in the brain, or by stimulating neurons through electrical impulses. The neurons that can be grown on diamond act in place of nerves damaged through illness or injury (see section 1.5.4) and so in order for the implanted electrodes to function effectively, prolonged neuron growth must be sustained. Mature neurons are difficult to isolate, so the ability to grow specialised neurons from a stem cell culture is vital. hIPS are of specific interest as they best represent the neuronal differentiation observed in human development.

### 1.5.1 - Electrode Activity

A main issue that surrounds the development of implanted electrodes is the reduction in performance over an extended period of time. Previous studies of non-diamond electrodes implanted in animals have shown that over six months there is a reduction of 40-60% in the quantity of active electrodes.<sup>38-40</sup>

This is due to the actual material that is currently implanted into the central nervous system which activates an immune response, causing an accumulation of cells about the foreign body. This response is termed glial scarring and is an important mechanism involved in the repair of the blood-brain barrier, an important biological structure that serves to protect the brain extracellular fluid from circulating blood and the possibility of bacterial infection.<sup>41, 42</sup> This glial scarring process leads to the encapsulation of any implanted electrode which ultimately reduces the activity of the implant.

By creating a surface that mimics the extracellular matrix it is hoped that the cytotoxic response from the body will be reduced, leading to a successful implantation of NCD.<sup>43</sup> Currently, the cationic polymer poly-L-lysine (PLL) is widely used as a coating that provides these conditions and optimises cell growth.<sup>44, 45</sup> However, PLL cannot be implanted into the body due to the activation of an immune response, thus for *in vivo* studies to be carried out, a substitute must be developed.<sup>46</sup>

#### 1.5.1.1 - Amine Functionalised Surface

Hopper *et al.* produced an amine-functionalised hydrogenated nanodiamond coating as an alternative to PLL.<sup>47</sup> Through irradiation with UV light, hydrogen terminated NCD was functionalised by fixing trifluoroacetic acid protected 10-aminodec-1-ene (TFAAD) to the surface. This cationic amine functionalised NCD (AmNCD) was then stabilised by being deposited onto acrylic acid plasma polymer coated glass (AANCD).

To assess the ability of cell growth, NG108-15 neuroblastoma-glyoma hybrid cells were cultured on AANCD, glass (negative control), acrylic acid plasma polymer coated glass (AA) and PLL (positive control).

As seen in Figure 1.5.1.1, all surfaces adhered and grew the neuroblastoma cells after seven days in culture. There is significant difference in the morphologies between the surfaces. The negative control, glass, shows a round morphology of cells which contrast with the fluorescence images

obtained of PLL coated glass and AANCD. PLL coated glass and amine functionalised NCD show considerable extensions of the cells, suggesting neurite-like behaviour has been achieved in these cases. Growth on AA suggests a higher proliferation rate of cells; however, there is reduced neurite extension expressed in the images, implying that AA does not successfully support the growth of NG108-15.

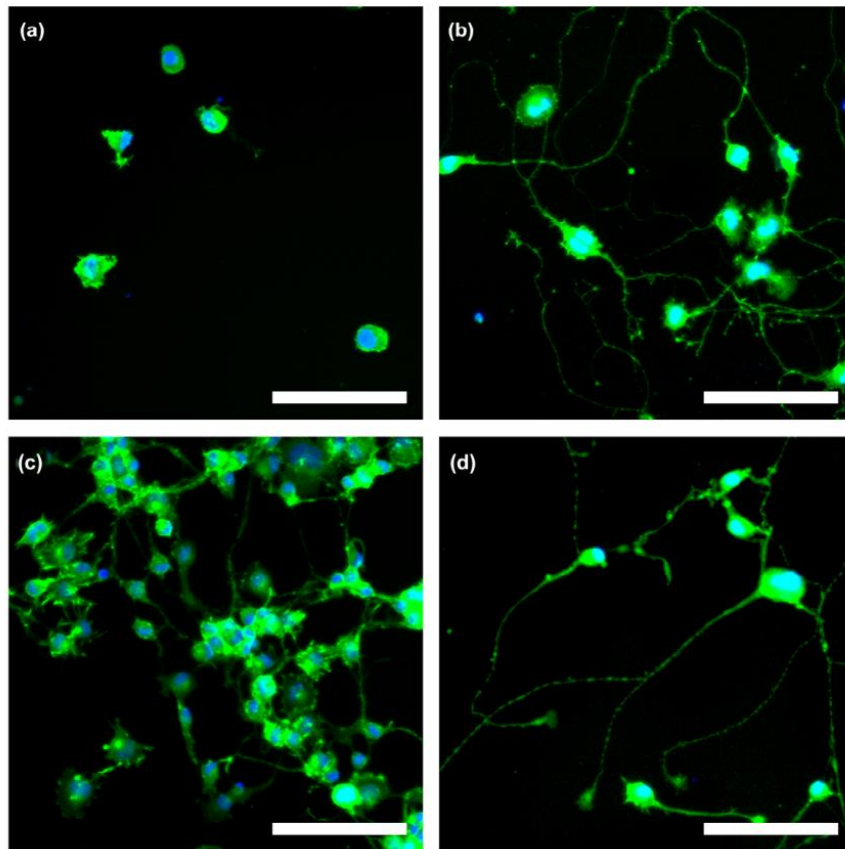


**Figure 1.5.1.1:** Fluorescence micrographs of NG108-15 cells after 7 days culture. Stained for f-actin (green) and nuclei (blue). (a) Cells grown on glass. (b) Cells grown on poly-L-lysine coated glass. (c) Cells grown on acrylic acid plasma polymer coated glass. (d) Cells grown on amine functionalised NCD deposited on acrylic acid plasma polymer glass.<sup>47</sup>

In accordance with Figure 5.1.1a, data showed that after seven days the surface coated in AANCD and PLL had grown the largest number of neurites amongst all four surfaces, with the total number of each corresponding well to each other. PLL grew slightly longer neurites, though this is reported as statistically insignificant. This implied that AANCD was a successful material to grow the NG108-15 cell line which could have an impact on future cell-growth studies that are dependent on PLL.

### 1.5.2 - Electrode Capacitance

It has been noted that planar B-NCD exhibits low capacitance, meaning the activity of the electrode made from this material will be significantly reduced. To overcome this, the surface area of the diamond is required to increase and this can be achieved through nanostructuring of the diamond surface.<sup>48</sup>

### 1.5.2.1 - Surface Structuring *via* Carbon Nanotubes

Taylor *et al.* investigated the use of carbon nanotubes (CNT) to act as a scaffold on which NCD could then be coated on to.<sup>49</sup> The report investigated the comparisons of growth of hNSCs on oxygen-terminated substrates that expressed different topologies of diamond, including un-doped NCD and B-NCD-CNT structures, and tissue culture polystyrene (TCPS) to act as a control.

CNT heights of 1  $\mu\text{m}$  and 2  $\mu\text{m}$  were assessed and it was found that the shorter nanotubes led to a density of 9  $\mu\text{m}^{-2}$  for bundles produced, whereas the density for the longer nanotubes saw a decrease to 4  $\mu\text{m}^{-2}$ .

Once hNSCs were seeded onto the TCPS, NCD, B-NCD, and nanostructured surfaces, the adhesion capability of the cells on all planar substrates were measured by immunohistochemical imaging. The morphology and proliferation rates of cells on planar NCD and B-NCD structures were found to be consistent with hNSCs growing on the control TCPS, suggesting planar NCD and B-NCD were as suitable as TCPS to grow neural cells on.

The survivability of the cells on all substrates was measured by methylene blue assay. Whilst planar NCD and B-NCD showed a lower cell count in comparison to TCPS, both nanostructured B-NCD substrates led to a significant increase in cell count. The increase of B-NCD CNTs from 1  $\mu\text{m}$  to 2  $\mu\text{m}$  resulted in an increase of cell adhesion and count, suggesting that carbon nanotube scaffolds have a significant effect on the growth of neurons.

A further investigation revolving around 3D structuring *via* CNTs was led by Piret *et al.*<sup>48</sup> Cells isolated from the hippocampi and spinal cords of mice were shown to grow equally as well on the 3D nanostructured BDD surfaces as conventional 2D BDD substrates. Scanning electron microscope images of these two surface types are shown in Figure 1.5.2.1.

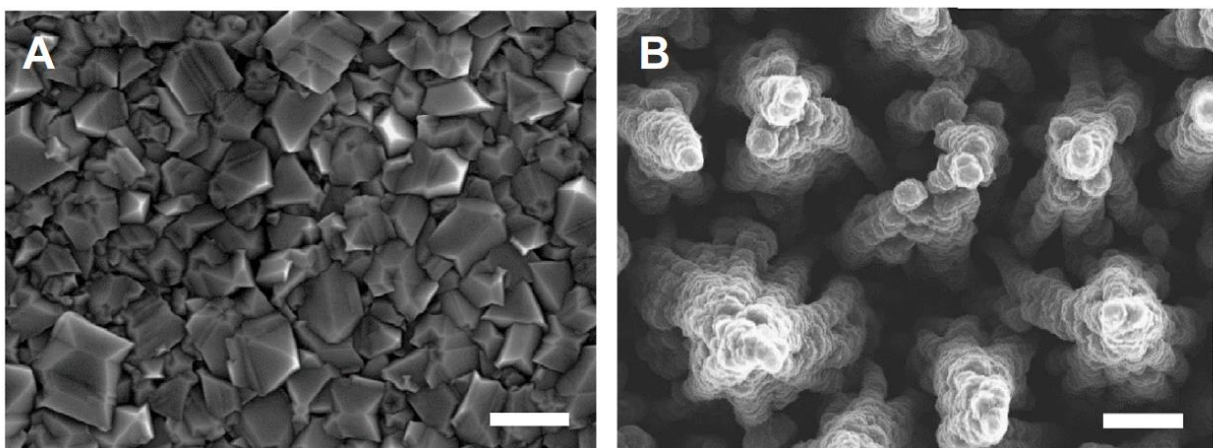


**Figure 1.5.2.1:** Scanning electron microscopy (SEM) of normal BNCD (A) and nanostructured BNCD (B). Scale bar, 600 nm.<sup>48</sup>

Microelectrode arrays were created from these substrates, and it was shown that the impedance values of the 3D BDD arrays were 40 times less than those incorporating planar BDD. The structuring also allowed for recording of low amplitude signals (10-20  $\mu\text{V}$ ) which were not recorded reliably by standard 2D BDD microelectrodes.

The use of CNTs for biomedical applications may be limited by their apparent toxicity. Studies have shown that CNTs may potentially have a harmful effect on the body, although there are a number of controversies surrounding this. The toxicity or biocompatibility of CNTs must be proven beyond doubt before their implementation.<sup>50,51</sup>

### **1.5.3 - Guided Cell Growth**

A further option of increasing the performance of electrodes is to spatially control the pathway neurons are grown on diamond. Neurons cultured on standard homogenous substrates tend to cluster and form random connections which can lead to difficulties in their analysis and subsequent improvement. By controlling the areas that neurons can grow, a route for the cells to extend along can be determined which can ultimately lead to a more specific electrode. Previous work has already shown that directed growth results in an increase in recorded signal-to-noise ratios (SNRs) on comparison with wire and silicon electrode arrays.<sup>52</sup> Therefore it is assumed that if the order of the neurons can be increased, the SNR will rise, leading to an electrode with superior performance.

#### **1.5.3.1 - Spatially Controlling Cell Growth**

There are a number of methods to control the pathway and projection of neurons, including the use of laser micro-machining, inkjet-printing, photolithography and micro-contact printing ( $\mu$ CP). Photolithography is a direct lithography method involving the etching of a silicon surface through the interaction of light with a patterned resist.<sup>53</sup>  $\mu$ CP is a soft lithography technique that has been shown to function through the absorption of the desired molecule to be printed onto a patterned template formed of a polymer. These molecules can then diffuse onto the substrate when it comes into contact with the stamp.<sup>54</sup> While simple enough in theory, there are practical issues that limit its usability. Most significant is that the patterned stamp is a physical entity and as such cannot be modified after creation. It is also less cost effective than photolithography for larger patterning applications.

##### **1.5.3.1.1 - Spatial Control *via* Inkjet Printing**

Inkjet-printing both offers the advantage of versatility over lithography techniques at some cost to the spatial resolution.<sup>55</sup> The programmability of this technique, along with exact reproducibility makes it a viable option for patterning cellular growth. Laser etching displays the same versatility as inkjet-printing but with higher resolutions. Regan *et al.* investigated both *in vitro* inkjet-printing and laser etching in the combined patterning of neurons and inflammatory cells (through anti-biofouling agents) to create a tailored coating for electrodes.<sup>56</sup>

It has been shown that PLL enhances neural cell adhesion to DLC doped with either phosphorus (P-DLC) or boron (B-DLC).<sup>57</sup> Inkjet printing was used in the deposition of 50  $\mu$ m spots of PLL onto P-DLC substrates and it was found that neurons adhered mostly to the PLL-printed areas in a monolayered fashion. The application of PLL printing on electrodes was also studied, through parallel PLL line deposition on a commercially available micro-electrode array. It was found that the majority of neuronal mass was formed along the 50  $\mu$ m x 400  $\mu$ m PLL lines, with only minimal growth in non-printed areas.

### 1.5.3.1.2 - Spatial Control *via* Laser Etching

Before testing the laser etching method, it was necessary to evaluate whether neurons would adhere to a PLL-coated BDD substrate. By comparison to undoped diamond and a polystyrene standard, it was found that neuron adhesion was unaffected. Laser etching of 100  $\mu\text{m}$  by 1000  $\mu\text{m}$  rectangles (10  $\mu\text{m}$  line width) on boron-doped diamond resulted in neurons showing good adhesion to the PLL-coated areas and avoidance of growth on the etched lines. This is most likely due to the destruction of the favourable PLL coating in these areas, although effects from a change in topology in the etched areas could be possible.

Using laser etching as a means to spatially control the growth of neurons was further explored by May *et al.* in a similar application of laser etching to a B-doped CVD diamond substrate coated with PLL.<sup>58</sup> The results corroborated the earlier laser patterning work, and it was found that neural adhesion was limited nearly exclusively to the non-etched PLL areas with close to zero adhesion and dendrite growth on laser etched areas. It was also noted that the substrate areas that were not etched were unaffected by the laser process and as such remained pristine. This can be seen below, in Figure 1.5.3.1.2.

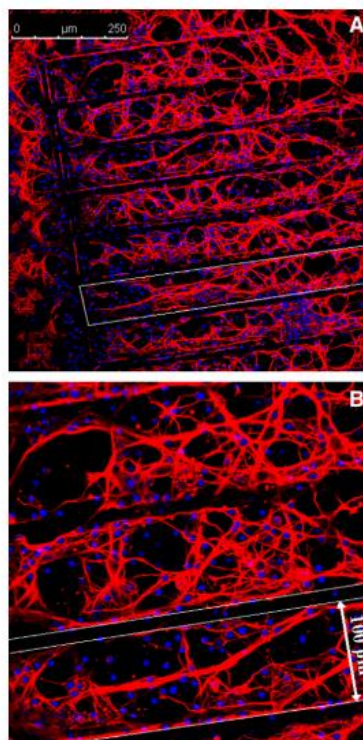


**Figure 1.5.3.1.2:** Fluorescence microscope images of neuron growth on O-terminated CVD diamond. The CVD diamond was laser patterned into 100  $\mu\text{m}$  by 1000  $\mu\text{m}$  rectangles, shown in (a) low magnification and (b) high magnification. Nuclei are stained blue and dendrite growth is stained red.<sup>58</sup>

### 1.5.3.2 - Diamond Coated Silicon Pillars

Cai *et al.* led an investigation into the effect of 3D patterning NCD on the growth of cells and this time, human auditory neurons were used.<sup>59</sup> This research came about from the interest in developing cochlear implants, whereby a 12-20 electrode array is used to replicate the function of 3400 inner hair cells. 5x5  $\mu\text{m}^2$  silicon pillars with NCD tops were fabricated, with a variety of inter-

pillar distances ranging from 4  $\mu\text{m}$  to 14  $\mu\text{m}$ . Due to the anatomical difficulty involved in isolating the cells of interest, only the flat NCD and 4  $\mu\text{m}$  spaced pillar topology were characterised.

It was found that the neurons did not adhere well to a flat NCD surface, but adhesion was significantly higher on NCD surfaces with inter-pillar distances of 4  $\mu\text{m}$ . The neuron growth was guided on these structured surfaces, as it was seen that the neuron growth was strictly observed along the tops of the pillars, along with no growth seen after the edge of the pillar landscape. These findings suggest that the NCD-topped pillar formation may prove useful in the design of future cochlear implants due to the extra adhesion and guided neuron growth in tandem with the conductive possibilities afforded by boron doping.

Further investigation into the effects of 3D substrate structure can allow for deeper understanding of how the cells would grow in their normal environment. Standard culturing in two dimensions is not fully representative of this environment and so Kaivosoja *et al.* experimented with substrates containing 3D diamond-like carbon micropillars. They hypothesized that this structuring would elongate the cytoskeleton and therefore promote osteogenesis (the formation of bone).<sup>60</sup> The 3D pillar landscape was formed by deposition of the DLC onto a patterned silicon mask. A control planar substrate was compared with surfaces covered in 100  $\mu\text{m}$  by 100  $\mu\text{m}$  pillars with heights of 200 nm, 5  $\mu\text{m}$  and 20  $\mu\text{m}$ . The adhesion and proliferation of osteoblastic SaOS-2 cells, fibroblasts and mesenchymal stem cells were studied.

Osteogenesis was monitored after 14 days by alkaline phosphatase (ALP) staining. ALP activity on the planar and 200 nm pillar substrates was random, indicating no interference from the low level pillar. For the 5  $\mu\text{m}$  pillar surface, staining was found most strongly in the interspace between pillars, although some staining was present on top of the pillars. In the 20  $\mu\text{m}$  pillar landscape there was, again, strong staining in the interspace but now almost no staining on top of the pillars, as can be seen in Figure 1.5.3.2.

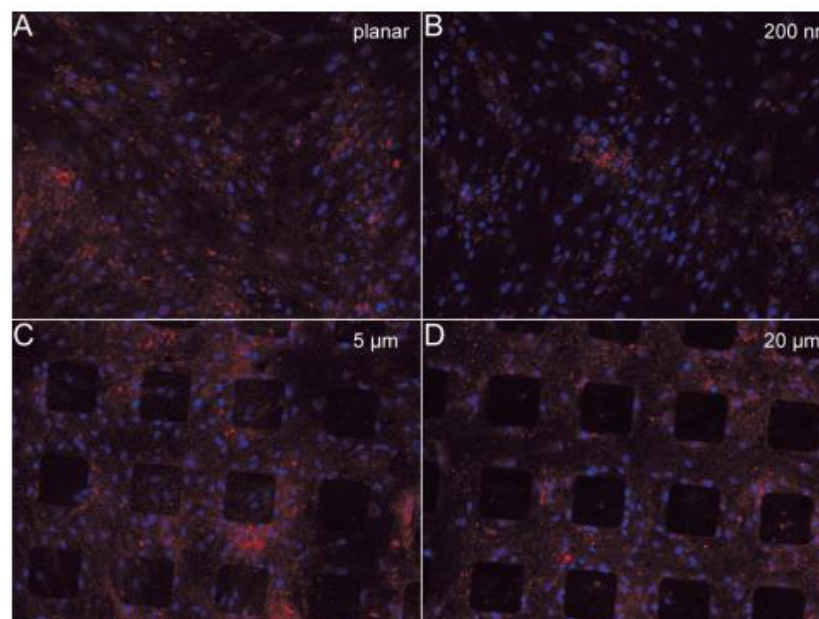


**Figure 1.5.3.2:** ALP staining (shown in red) of MSCs (nuclei shown in blue) grown on (a) planar DLC coated silicon and (b to d) on DLC coated Si with pillar arrays of heights 200 nm, 5  $\mu\text{m}$  and 20  $\mu\text{m}$  respectively.<sup>60</sup>

While elongation of the cytoskeleton did occur, it did not lead to significant increase of osteogenesis. Osteopontin (a protein found in bone) expression was enhanced somewhat for the 5  $\mu\text{m}$  and 20  $\mu\text{m}$  pillar substrates, although it was hypothesized that the 20  $\mu\text{m}$  pillar landscape limited cell-cell contact and therefore decreased osteogenesis.

#### **1.5.4 - Future Prospects**

The need for the increased performance of electrodes through the spatial control of neuron growth, surface functionalization and 3D structuring arises from the implementation of such electrodes in arrays for brain-computer interfaces (BCIs). A BCI allows for direct communication between the brain and a computer. Logical applications of these BCIs include restoring motor function, to those suffering from neuromuscular disorders, and even restoration of eyesight to those with degenerative eye conditions.

*In vivo* studies of diamond coated implants are still limited, due to problems arising from aforementioned issues such as glial scarring. This has meant that the use of diamond in BCIs has not yet been fully explored and has not been implemented into applications, such as the BrainGate project, where the use of diamond implants could provide a significant development.

##### **1.5.4.1 - BrainGate project**

The BrainGate project is dedicated to research into the improvement of BCI technology to aid recovery of functions lost through neurological disease. One such example of their work is the implanted 96-channel electrode array that allowed two separate participants, each with tetraplegia (no limb function) and anarthria (loss of speech), to demonstrate grasp and reach technique through a BCI controlled robotic arm.<sup>61</sup> While these movements were not as accurate or quick as an unimpaired individual, the ability to consciously perform these actions is a giant leap and further developments can lead to more rapid and dextrous movement. More recently, the BrainGate project reported on the increasing speed and reliability of BCIs for use in communications. The problems with long term robustness, however, remain.<sup>62</sup>

##### **1.5.4.2 - Retinal Prosthetics**

There have been many investigations into retinal prostheses, which can be split into two categories; subretinal and epiretinal. Subretinal implants are implanted on the outer retinal layer and designed to stimulate other, intact, retinal layers. Epiretinal implants are placed on the inner retina surface and communicate directly with ganglion cells (retinal neurons). A subretinal implant, with 16 electrodes, has been shown to allow patients to distinguish letters, while an epiretinal system, with 60 electrodes, has become the world's first retinal implant to be approved by the Food and Drug Administration (FDA).<sup>63, 64</sup> It has been suggested that it may take up to 1000 electrodes to achieve the spatial resolution necessary for tasks such as facial recognition and normal reading.<sup>65</sup>

Ganesan *et al.* demonstrated the application of diamond as an electrode array designed for this use in retinal prosthetics, and this work was improved upon by Bendali *et al.* who introduced new methods in the development of a 3D array with increased electrode density.<sup>66, 67</sup> This increased electrode density could lead to improved retinal implants, dependent on the use of diamond.

The potential applications for diamond as a substrate for cell growth are of huge importance, as is described in the select examples above, and it is therefore crucial that more research is undertaken to fully develop these ideas.

## 2 - Experimental - Developing Diamond Patterning Techniques

### 2.1 - Aims and Objectives

Developing methods of patterning diamond is of increasing necessity for applications such as the ability to control the growth of neurons. As seen in section 1.5.3, the study of controlled growth of neurons on diamond is of great importance as it offers the potential to counter several medical complications.

The aim of this project was to explore a new avenue of diamond patterning techniques. An investigation was conducted into the method of patterning diamond by attempting to produce tracks of diamond on a silicon substrate. This process is summarised in Figure 2.1.

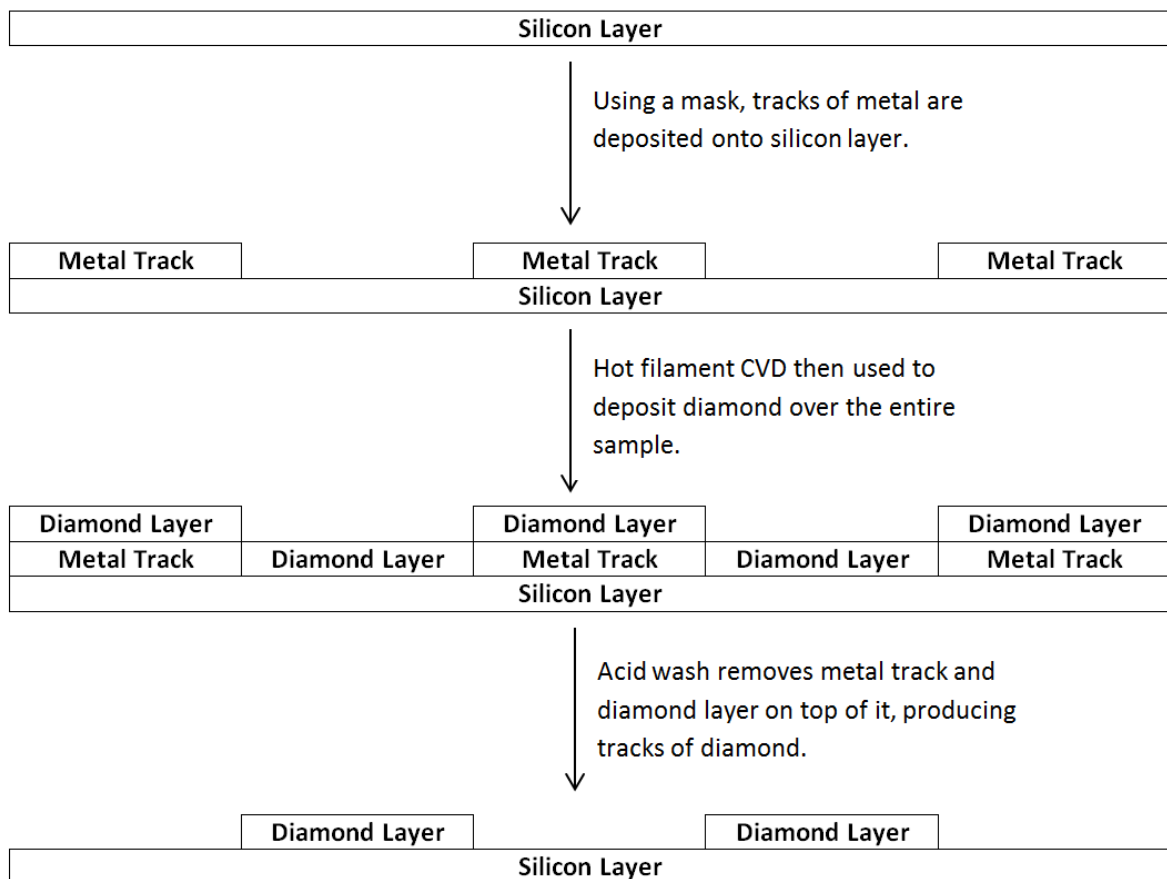


**Figure 2.1:** Diagram to show the proposed method of patterning diamond.

This design would confine neuron growth to along the diamond tracks only, thus controlling the extension of the neurons. The metals used in this project were gold and then copper.

## 2.2 - Method and Materials

### 2.2.1 - Gold (Sample A)

To create gold tracks on the silicon surface, a bell jar evaporator (Edwards E306 Belljar Evaporator) was used to evaporate a sample of gold foil onto silicon samples through a premade mask. The mask produced three gold tracks of 100  $\mu\text{m}$  width onto the surface of the silicon, as shown in Figure 2.2.1a.

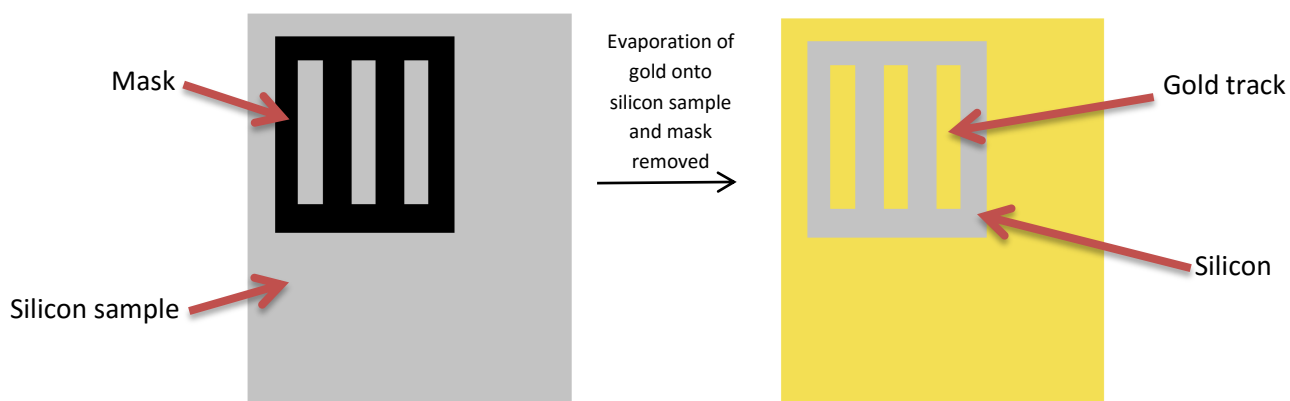


**Figure 2.2.1a:** Diagram generated to summarise steps involved with evaporating gold onto silicon sample through a mask.

The samples were then seeded *via* a carboxyethylsilanetriol sodium salt (25% in water) solution and 18-36 nm diamond suspension. A hot filament CVD reactor using tantalum filaments produced a boron-doped diamond film. The CVD reactor was operated under the following conditions: 1%  $\text{CH}_4$  in  $\text{H}_2$ , approx. 2000 ppm diborane, 20 Torr, 25 A supplied to filaments, 4 A supplied to substrate heater. The hot filament reactor grew the diamond over the period of one hour. To remove the layer of gold, and diamond layer above the metal, the sample was washed with Aqua Regia. Aqua Regia is typically a 1:3 molar mixture of concentrated nitric acid to concentrated hydrochloric acid and is a common medium to dissolve gold (equation 2.2.1).<sup>68</sup>



Using an enclosed Nd:YAG laser (Alpha, Oxford Lasers), a laser was used to create four holes near the corners of the tracks (Figure 2.2.1b). These holes were created to assist in locating the tracks when using the SEM.

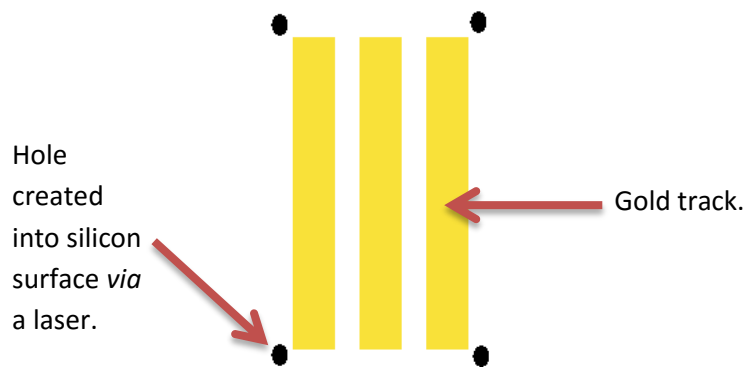


**Figure 2.2.1b:** Diagram generated to show the location of holes created *via* a laser into the silicon surface.

Finally, the samples were characterized by the use of a scanning electron microscope (Jeol IT300 SEM).

## 2.2.2 - Copper

### 2.2.2.1 - Copper Tracks on Silicon, Aqua Regia (Sample B)

Copper tracks were deposited onto a silicon sample *via* the same process as described in section 2.2.1, however using copper wire in place of gold foil in the bell jar evaporator. The samples were cleaned for 15 minutes *via* hydrogen plasma created in a microwave CVD reactor. Cleaning *via* hydrogen plasma was employed to avoid unwanted reactions between the copper and an acid wash. Following the same procedure as in section 2.2.1, four holes were created in the corners of the tracks before the samples were seeded and diamond was deposited over the sample *via* the hot filament CVD reactor using the same conditions as in section 2.2.1. The sample was then cleaned with Aqua Regia before being characterized by SEM.

### 2.2.2.2 - Copper Tracks on Silicon, No Aqua Regia (Sample C)

This sample was prepared *via* the same procedure as section 2.2.2.1, however no Aqua Regia was used to clean the sample at the last stage. Samples were characterized *via* SEM.

### 2.2.2.3 - Copper Layer on Silicon, No Aqua Regia (Sample D)

A bell jar evaporator was used to evaporate a layer of copper over an entire silicon sample. The sample was then cleaned *via* hydrogen plasma in a MWCVD reactor for 15 minutes. The samples were seeded and diamond was deposited onto the surface *via* HFCVD using the same conditions as in section 2.2.1. The sample was then analysed by SEM.

### 2.2.2.4 - Copper Layer on Silicon, No CVD (Sample E)

A bell jar evaporator was used to evaporate a layer of copper over an entire silicon sample. The sample was then cleaned *via* hydrogen plasma in a MWCVD reactor for 15 minutes. The sample was then cleaned with Aqua Regia and analysed by SEM.

## **2.3 - Results and Discussion**

### **2.3.1 - Gold**

The first material used in this method of patterning the diamond was gold. SEM pictures obtained at this stage were of low quality, however it could be seen that a layer of continuous crystalline diamond had formed on the surface. This film of diamond extended over the area the gold tracks were deposited, suggesting that the acid wash had had no effect on removal of the gold tracks and corresponding diamond layer. If the acid wash had been successful in removing both the gold and the diamond layer, the SEM images would show solid black tracks to signify the bare silicon layer. This process is reflected in Figure 2.1.

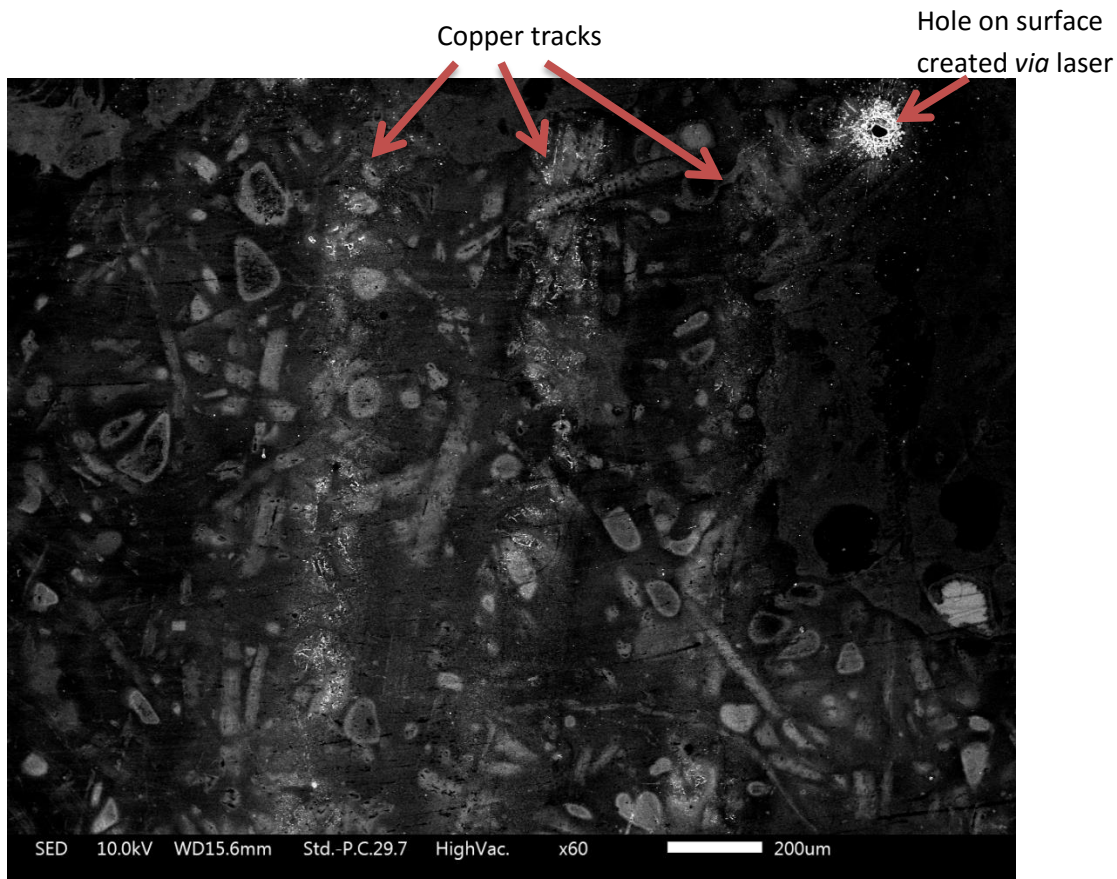
Due to the inability of the acid wash to remove the gold, the diamond remained non-patterned and as such, gold was deemed unsuitable for further investigation.

### **2.3.2 - Copper**

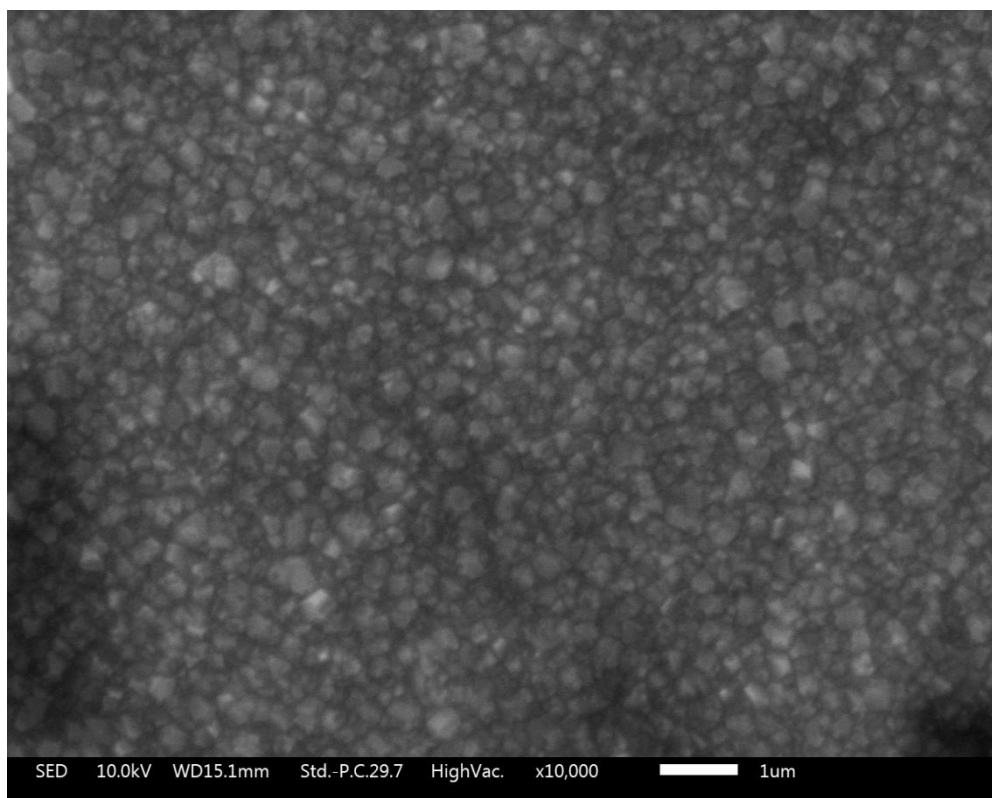
As gold proved to be inadequate for the patterning of diamond, copper was chosen as next material to investigate. Articles report that properties of copper, such as the thermal expansion coefficient and low carbon affinity, are not comparable to those of diamond and this leads to a weak adhesion between the diamond and the copper.<sup>69,70</sup> It was therefore hypothesized that the adverse conditions presented by copper would lead to a more disrupted growth of diamond over the copper tracks, causing the Aqua Regia wash to be more effective at removing the copper, and therefore, diamond layer than in comparison with gold.

Figure 2.3.2a shows that the process to create Sample B successfully imparts faint tracks onto the surface of silicon. This production of track markings indicates that copper is a more suitable material for this process in comparison with gold. This is due to the fact that previous samples using gold did not create any visible track markings when observed with SEM.

There are significant markings on the surface of Sample B which were thought to have occurred during the cleaning process with hydrogen plasma.



**Figure 2.3.2a:** SEM image of Sample B - diamond film grown over copper tracks on a silicon substrate washed with Aqua Regia. Diamond was deposited by CVD for one hour. SEM image at x60 magnification.



**Figure 2.3.2b:** SEM image of Sample B - diamond film grown on a silicon substrate washed with Aqua Regia. Diamond was deposited by CVD for one hour. SEM image at x10,000 magnification.

Figure 2.3.2b shows a magnified section of Sample B, highlighting an area of diamond growth directly onto the silicon substrate. The crystalline structure shows that diamond has been successfully deposited outside of any tracks.

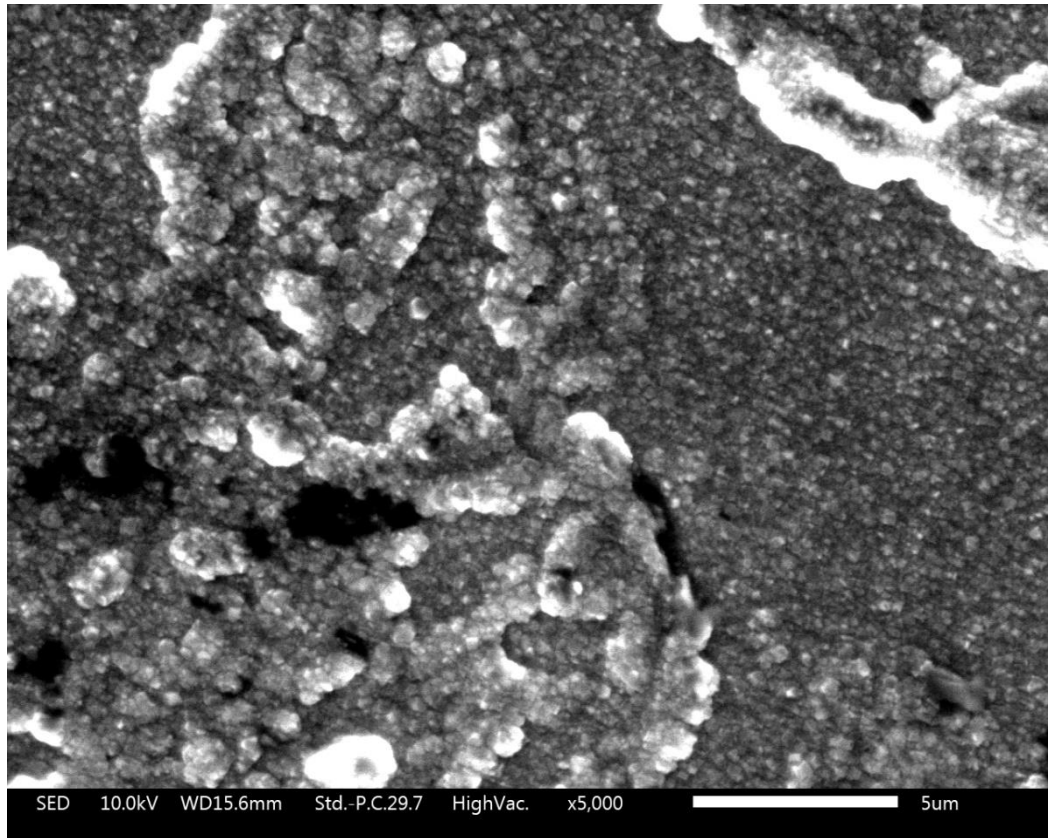


**Figure 2.3.2c:** SEM image of Sample B - diamond film grown over copper tracks on a silicon substrate washed with Aqua Regia. Diamond was deposited by CVD for one hour. SEM image at x5,000 magnification.

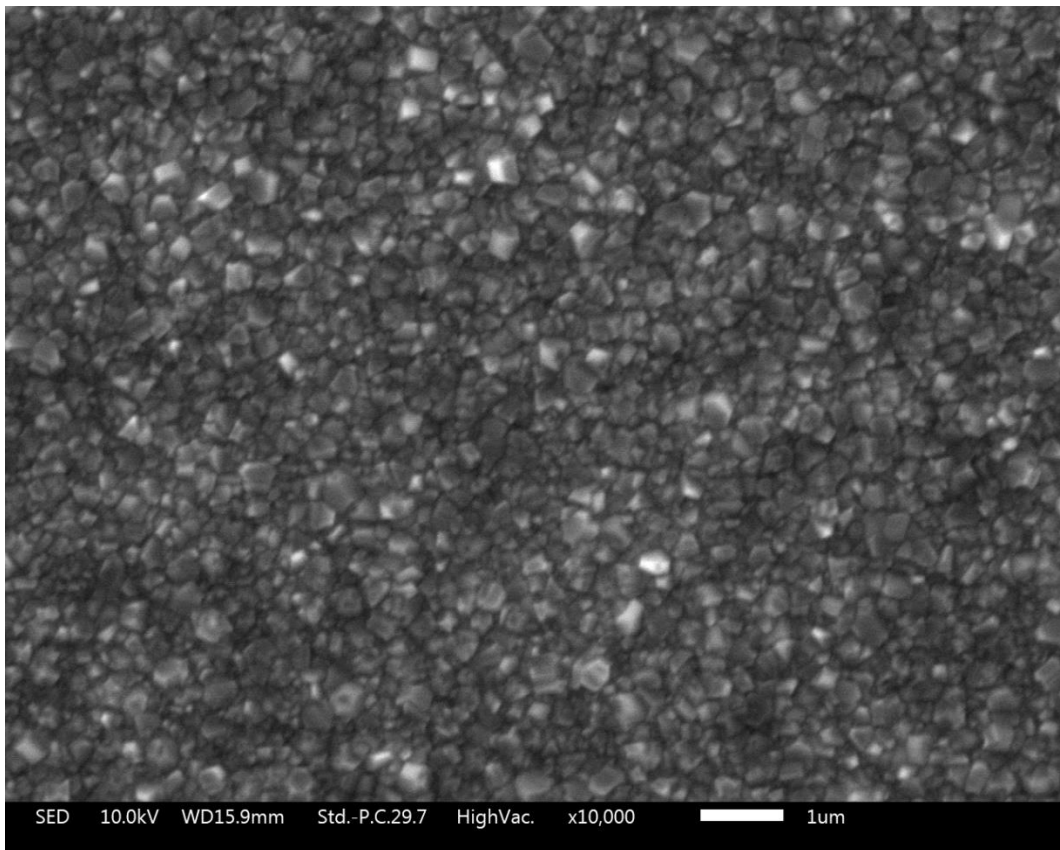
Figure 2.3.2c shows another magnified section of Sample B, highlighting an area of diamond growth on a copper track present on the silicon surface. This image of diamond structure within a track shows significant disruption of diamond growth in comparison with Figure 2.3.2b which shows continuous diamond growth outside of the tracks. Figure 2.3.2c shows several black areas which suggest that a proportion of the copper and diamond layer have been removed, revealing the silicon layer below.

The disruption here is much greater than in the previous gold samples, where a continuous diamond layer was present in the tracks. The increased hindrance to diamond growth shown in Figure 2.3.2c makes copper a more viable candidate than gold for this method of diamond patterning.

Figure 2.3.2c clearly shows that the majority of diamond still remains on the copper track, suggesting that the process has not been successful in removing the copper and diamond layers to produce

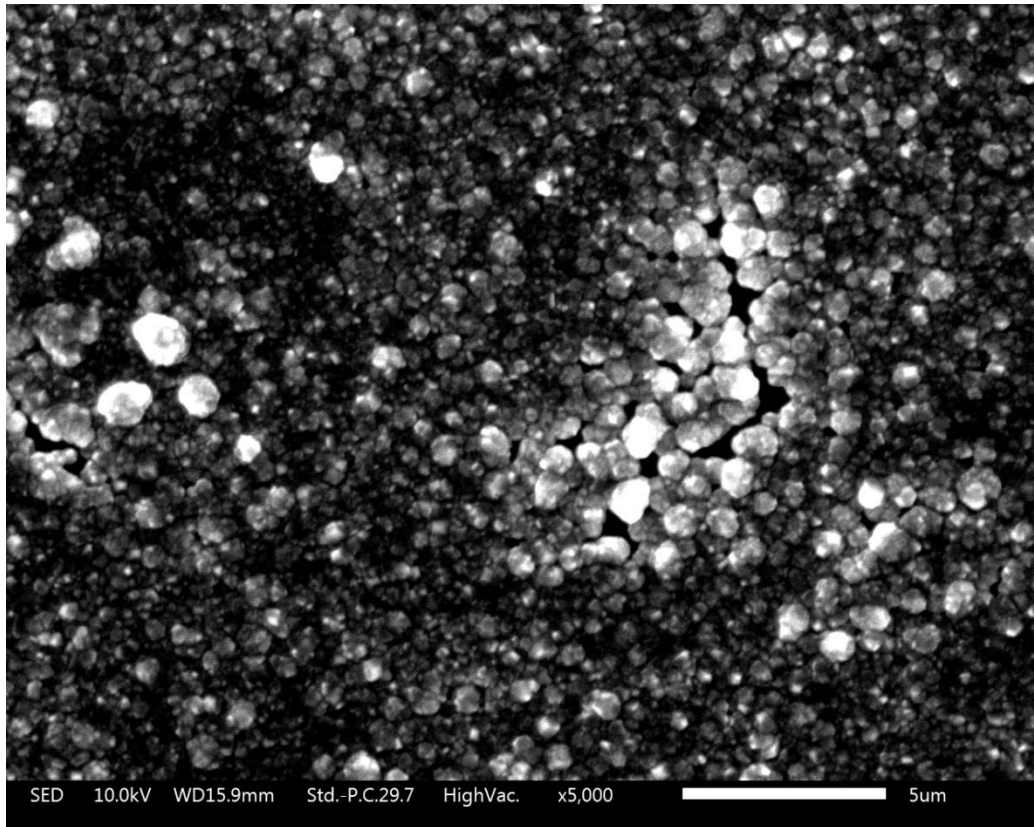
patterned diamond. Ultimately this means that the use of copper described in this diamond patterning technique is not effective.

Figure 2.3.2d shows a SEM image of Sample C, focusing on an area of diamond growth directly onto the silicon substrate. The crystalline structure shows that diamond has been successfully deposited outside of any tracks.



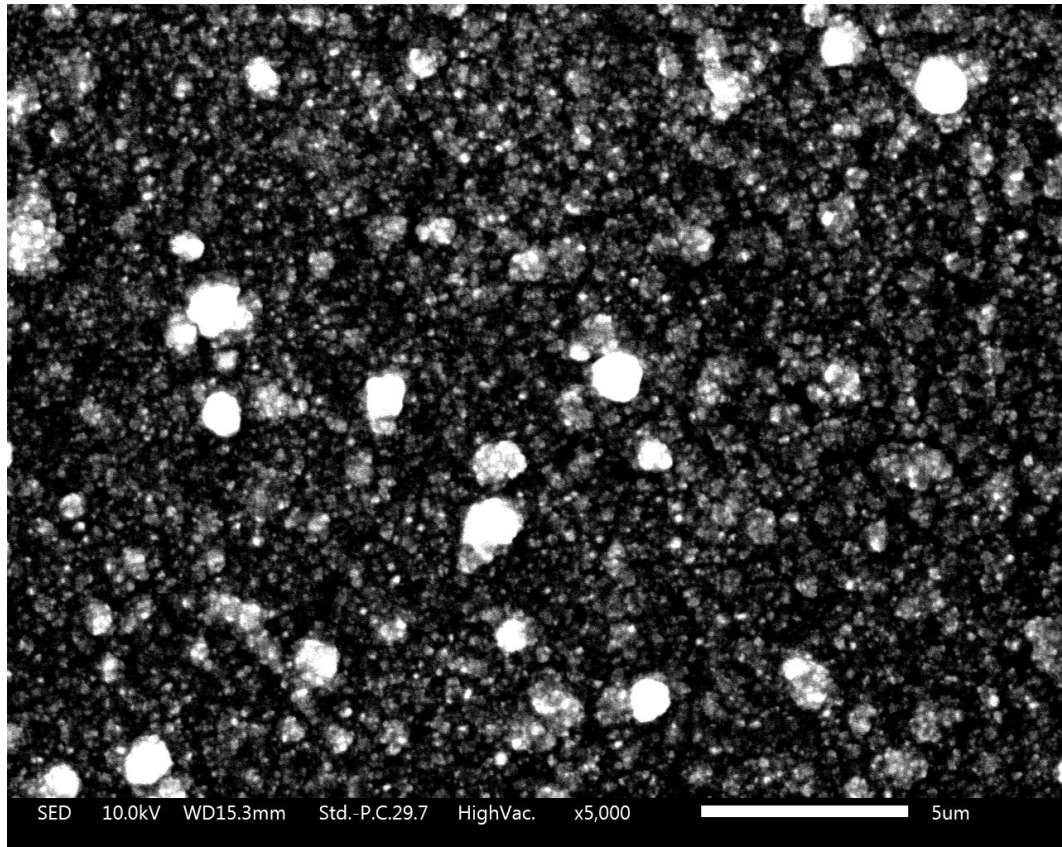
**Figure 2.3.2d:** SEM image of Sample C - diamond film grown on a silicon substrate. Diamond was deposited by CVD for one hour. SEM image at x10,000 magnification.

In comparison with Sample B, Sample C was not treated with Aqua Regia. Despite this difference, the diamond structures observed for both Sample B (Figure 2.3.2b) and Sample C (Figure 2.3.2d) in non-track areas are very similar. This suggests that the Aqua Regia treatment has little, if any, structural impact on the diamond film deposited directly onto the silicon substrate.



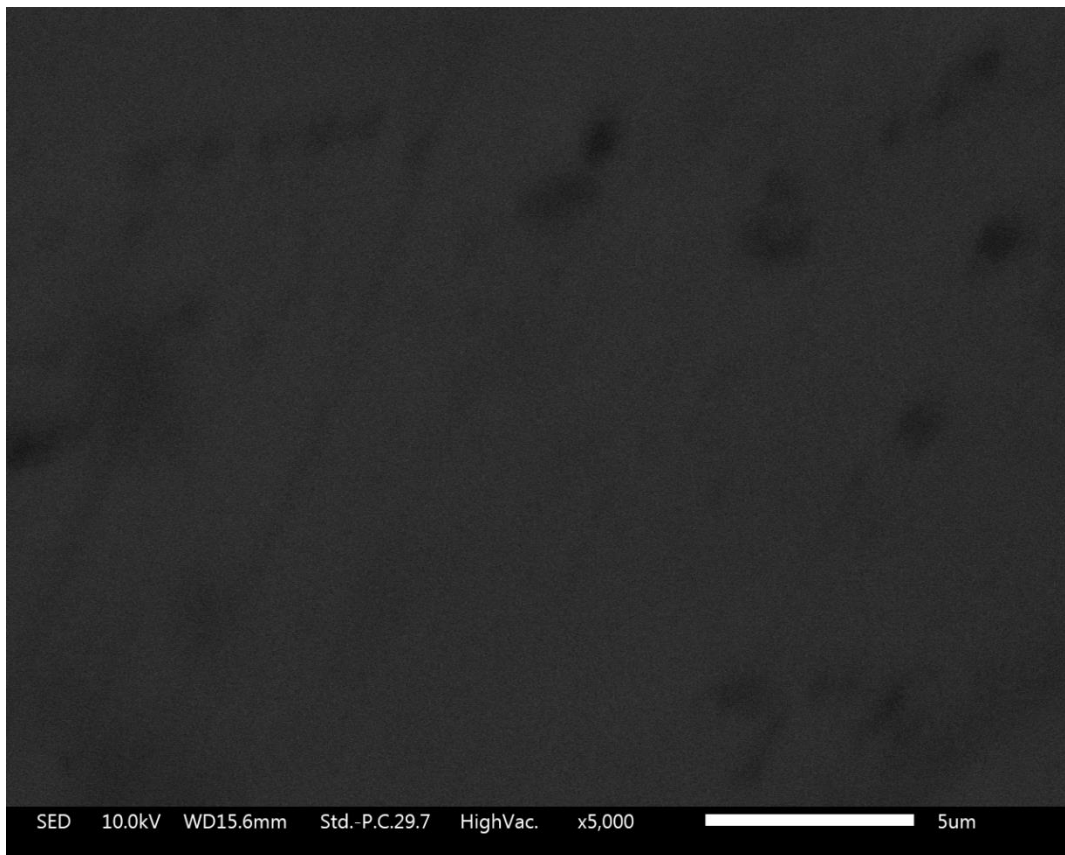
**Figure 2.3.2e:** SEM image of Sample C - diamond film grown over copper tracks on a silicon substrate. Diamond was deposited by CVD for one hour. SEM image at x5,000 magnification.

Figure 2.3.2e shows a magnified section of Sample C, where diamond has been grown on a copper track present on the silicon surface. This image shows that the diamond growth on copper has been disturbed even without addition of Aqua Regia. However, the diamond in Figure 2.3.2e is less disturbed than the corresponding copper track in Sample B (Figure 2.3.2c). This suggests that the addition of Aqua Regia does have some effect on the diamond structure but only when said diamond is grown on a copper track.



**Figure 2.3.2f:** SEM image of Sample D - diamond film grown on over a copper layer on a silicon substrate. Diamond was deposited by CVD for one hour. SEM image at x5,000 magnification.

Figure 2.3.2f shows an image of Sample D, where diamond film has been grown over a copper layer on a silicon surface. Now that the copper is not confined to a track, as in Sample C (Figure 2.3.2e), there is widespread disruption to the diamond structure. Again this is without the addition of Aqua Regia. This confirms that the copper layer is causing some level of disruption to the diamond growth.



**Figure 2.3.2g:** SEM image of Sample E - copper layer on a silicon substrate treated with Aqua Regia resulting in a bare silicon surface. SEM image at x5,000 magnification.

Figure 2.3.2g shows an image of Sample E, where no diamond was deposited onto the copper layer on the silicon surface. As Figure 2.3.2g shows only bare silicon, this demonstrates that the Aqua Regia treatment is entirely able to remove the copper layer on a silicon surface. However, as shown in Figure 2.3.2c this treatment is not effective when a diamond layer has been deposited on top of the copper.

## 2.4 - Conclusion

This project set out to develop a method for patterning diamond using a metal base layer. The evidence presented in section 2.3.1 showed that gold was an unsuitable candidate for this process as it had negligible effect on the structure of the diamond deposited across the surface.

Copper was used as an alternative to gold, as described in section 2.3.2, and was found to induce some level of disturbance in the diamond structure. This disturbance was enhanced by treatment with Aqua Regia, but the disturbance was not sufficient to cause patterning of the diamond.

Further study in this area of diamond patterning could see different metals used. A previous report has observed that molybdenum covered by gold has prevented the growth of diamond over this dual layer.<sup>71</sup> Further to this, molybdenum is soluble in an Aqua Regia solution so a molybdenum-gold track could be applied to the existing process.<sup>72</sup>

A change in the order the procedure is carried out could also be considered. By moving the diamond seeding step to before the evaporation of the metal onto the silicon sample, it is possible there will be little or no growth of diamond on the surface of the metal. This could lead to more facile removal of the metal tracks *via* an acid wash. Figure 2.4 summarises this proposed alteration.

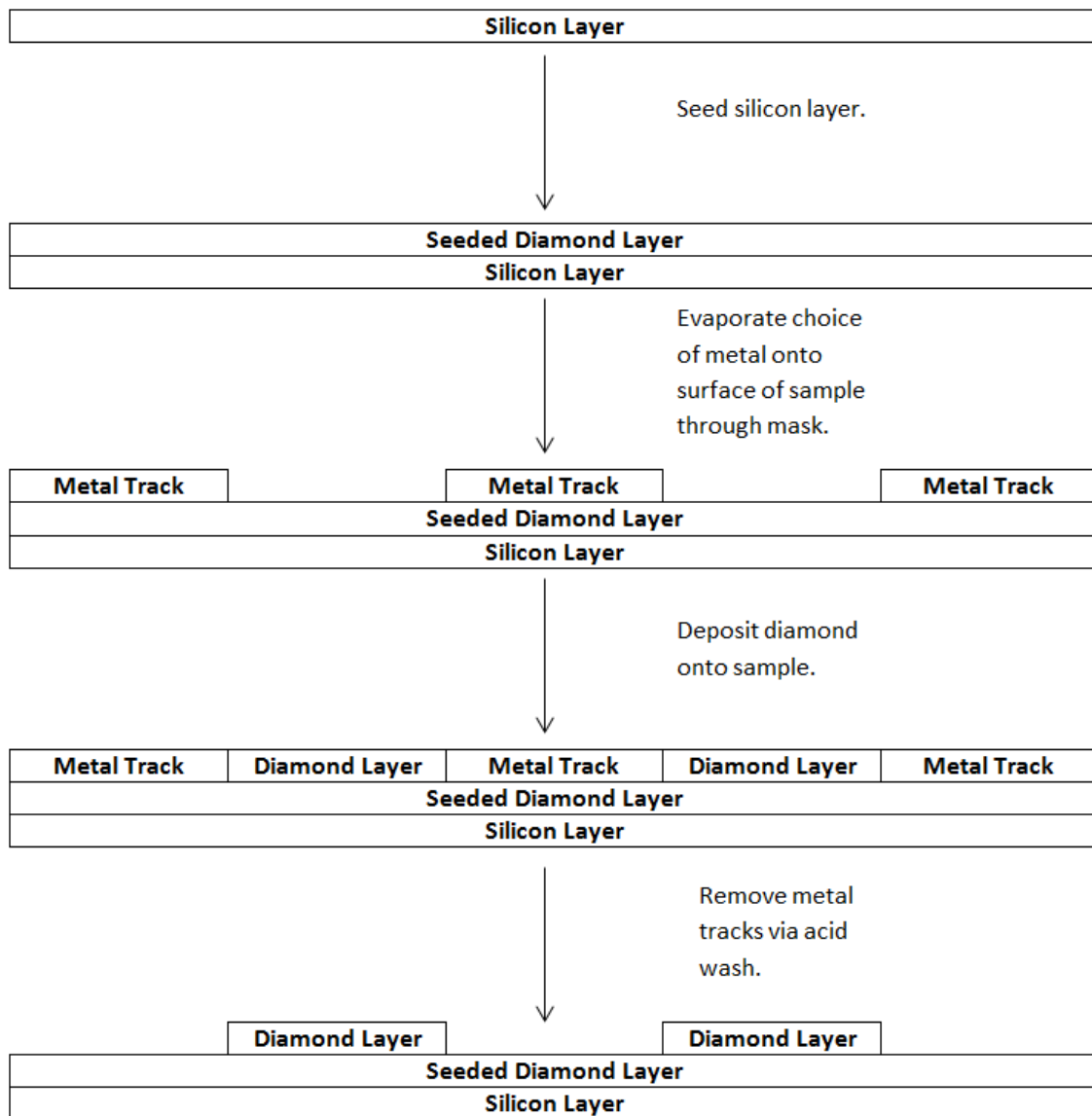


**Figure 2.4:** Diagram to show the altered method of patterning diamond.

Currently the methods detailed by this thesis are not powerful enough to replace existing patterning methods, but with further investigation they may well prove to be useful.

### 3 - References

1. P. W. May, Diamond, <http://www.bris.ac.uk/Depts/Chemistry/MOTM/diamond/diamond.htm>, (accessed November, 2015).
2. K. E. Spear and J. P. Dismukes, *Synthetic Diamond - Emerging CVD Science and Technology*, John Wiley & Sons, New York, 1994.
3. F. P. Bundy, H. T. Hall, H. M. Strong and R. H. Wentorf, *Nature*, 1955, **176**, 51-55.
4. *U.S Pat.*, 3030187, 3030188, 1958.
5. B. V. Deryagin, D. V. Fedoseev, V. M. Lukyanovich, B. V. Spitsyn, A. V. Ryanov and A. V. Lavrentyev, *J. Cryst. Growth*, 1968 **2**, 380.
6. J. C. Angus, H. A. Will and W. S. Stanko, *Journal of Applied Physics*, 1968, **39**, 2915-&.
7. B. V. Deryagin, B. V. Spitsyn, L. L. Builov, A. A. Klochov, A. E. Gorodetskii and A. V. Smol'yanimov, *Dokl. Akad. Nauk. SSSR*, 1976, **231**, 333.
8. S. Matsumoto, Y. Sato, M. Kamo and N. Setaka, *Jpn. J. Appl. Phys.*, 1982, **21**, 183.
9. S. Matsumoto, Y. Sato, M. Tsutsumi and N. Setaka, *J. Mater. Sci.*, 1982, **17**, 3106.
10. M. N. R. Ashfold, P. W. May, C. A. Rego and N. M. Everitt, *Chemical Society Reviews*, 1994, **23**, 21-30.
11. P. W. May, *Philosophical Transactions of the Royal Society of London Series a-Mathematical Physical and Engineering Sciences*, 2000, **358**, 473-495.
12. P. K. Bachmann, H. J. Hagemann, H. Lade, D. Leers, F. Picht, D. U. Wiechert and H. Wilson, *Mater. Res. Soc. Symp. Proc.*, 1994, **339**, 267-277.
13. Y. Zhu, J. Li, W. Li, Y. Zhang, X. Yang, N. Chen, Y. Sun, Y. Zhao, C. Fan and Q. Huang, *Theranostics*, 2012, **2**, 302-312.
14. M. Amaral, A. G. Dias, P. S. Gomes, M. A. Lopes, R. F. Silva, J. D. Santos and M. H. Fernandes, *Journal of Biomedical Materials Research Part A*, 2008, **87A**, 91-99.
15. W. Jakubowski, G. Bartosz, P. Niedzielski, W. Szymanski and B. Walkowiak, *Diamond and Related Materials*, 2004, **13**, 1761-1763.
16. B. Rezek, L. Michalikova, E. Ukraintsev, A. Kromka and M. Kalbacova, *Sensors*, 2009, **9**, 3549-3562.
17. M. Kalbacova, M. Kalbac, L. Dunsch, A. Kromka, M. Vanecek, B. Rezek, U. Hempel and S. Kmoch, *Physica Status Solidi B-Basic Solid State Physics*, 2007, **244**, 4356-4359.
18. Y. Arima and H. Iwata, *Journal of Materials Chemistry*, 2007, **17**, 4079-4087.
19. R. S. Sussmann, *CVD Diamond for Electronic Devices and Sensors*, John Wiley & Sons Ltd, U.K, 2009.
20. V. S. S. Vadali, P. Sampath Kumar and V. B. Kumar, *International Journal of Electrochemistry*, 2012, **2012**.
21. G. Pastor-Moreno, Ph.D., University of Bristol, 2002.
22. K. F. Chong, K. P. Loh, S. R. K. Vedula, C. T. Lim, H. Sternschulte, D. Steinmuller, F.-s. Sheu and Y. L. Zhong, *Langmuir*, 2007, **23**, 5615-5621.
23. A. Vaitkuvienė, M. McDonald, F. Vahidpour, J.-P. Noben, K. Sanen, M. Ameloot, V. Ratautaite, V. Kasetė, G. Biziuleviciene, A. Ramanaviciene, M. Nesladek and A. Ramanavicius, *New Biotechnology*, 2015, **32**, 7-12.
24. F. Klauser, M. Hermann, D. Steinmueller-Nethl, O. Eiter, A. Pasquarelli, E. Bertel, T. Seppi, P. Lukas and T. Lechleitner, *Chemical Vapor Deposition*, 2010, **16**, 42-49.
25. B. Rezek, E. Ukraintsev, M. Kratka, A. Taylor, F. Fendrych and V. Mandys, *Biointerphases*, 2014, **9**.
26. L. Grausova, A. Kromka, L. Bacakova, S. Potocky, M. Vanecek and V. Lisa, *Diamond and Related Materials*, 2008, **17**, 1405-1409.
27. L. Bacakova, V. Stary, O. Kofronova and V. Lisa, *Journal of Biomedical Materials Research*, 2001, **54**, 567-578.

28. B. R. Chrcanovic, T. Albrektsson and A. Wennerberg, *Journal of Dental Research*, 2014, **93**, 859-867.
29. G. Heinrich, T. Grogler, S. M. Rosiwal and R. F. Singer, *Surface & Coatings Technology*, 1997, **94-5**, 514-520.
30. R. Pareta, L. Yang, A. Kothari, S. Sirinrath, X. Xiao, B. W. Sheldon and T. J. Webster, *Journal of Biomedical Materials Research*, 2010, **95**, 129-136.
31. H. Liu, E. B. Slamovich and T. J. Webster, *Journal of Biomedical Materials Research*, 2006, **78**, 798-807.
32. L. Yang, Y. Li, B. W. Sheldon and T. J. Webster, *Journal of Materials Chemistry*, 2012, **22**, 205-214.
33. P. Strąkowska, R. Beutner, M. Gnyba, A. Zielinski and D. Scharnweber, *Materials Science and Engineering*, 2015, **59**, 624-635.
34. W. C. Clem, S. Chowdhury, S. A. Catledge, J. J. Weimer, F. M. Shaikh, K. M. Hennessy, V. V. Kononov, M. R. Hill, A. Waterfeld, S. L. Bellis and Y. K. Vohra, *Biomaterials*, 2008, **29**, 3461-3468.
35. S. E. Duailibi, M. T. Duailibi, L. M. Ferreira, K. I. Ladislau Carvalho Salmazi, M. C. Salvadori, F. d. S. Teixeira, A. Pasquarelli, J. P. Vacanti and P. C. Yelick, *Tissue Engineering Part A*, 2013, **19**, 2537-2543.
36. Y.-C. Chen, D.-C. Lee, C.-Y. Hsiao, Y.-F. Chung, H.-C. Chen, J. P. Thomas, W.-F. Pong, N.-H. Tai, I. N. Lin and I.-M. Chiu, *Biomaterials*, 2009, **30**, 3428-3435.
37. P. A. Nistor, P. W. May, F. Tamagnini, A. D. Randall and M. A. Caldwell, *Biomaterials*, 2015, **61**, 139-149.
38. P. J. Rousche and R. A. Normann, *Journal of Neuroscience Methods*, 1998, **82**, 1-15.
39. M. A. L. Nicolelis, D. Dimitrov, J. M. Carmena, R. Crist, G. Lehew, J. D. Kralik and S. P. Wise, *Proceedings of the National Academy of Sciences of the United States of America*, 2003, **100**, 11041-11046.
40. J. C. Williams, R. L. Rennaker and D. R. Kipke, *Brain Research Protocols*, 1999, **4**, 303-313.
41. V. S. Polikov, P. A. Tresco and W. M. Reichert, *Journal of Neuroscience Methods*, 2005, **148**, 1-18.
42. J. Silver and J. H. Miller, *Nature Reviews Neuroscience*, 2004, **5**, 146-156.
43. R. M. Boehler, J. G. Graham and L. D. Shea, *Biotechniques*, 2011, **51**, 239-+.
44. B. G. Chung, L. A. Flanagan, S. W. Rhee, P. H. Schwartz, A. P. Lee, E. S. Monuki and N. L. Jeon, *Lab on a Chip*, 2005, **5**, 401-406.
45. E. Yavin and Z. Yavin, *Journal of Cell Biology*, 1974, **62**, 540-546.
46. D. Fischer, Y. X. Li, B. Ahlemeyer, J. Krieglstein and T. Kissel, *Biomaterials*, 2003, **24**, 1121-1131.
47. A. P. Hopper, J. M. Dugan, A. A. Gill, O. J. L. Fox, P. W. May, J. W. Haycock and F. Claeysens, *Biomedical Materials*, 2014, **9**.
48. G. Piret, C. Hebert, J.-P. Mazellier, L. Rousseau, E. Scorsone, M. Cottance, G. Lissorgues, M. O. Heuschkel, S. Picaud, P. Bergonzo and B. Yvert, *Biomaterials*, 2015, **53**, 173-183.
49. A. C. Taylor, B. Vagaska, R. Edgington, C. Hébert, P. Ferretti, P. Bergonzo and R. B. Jackman, *Journal of Neural Engineering*, 2015, **12**.
50. J. P. Kaiser, M. Reosslein, T. Buerki-Thurnherr and P. Wick, *Current Medicinal Chemistry*, 2011, **18**, 2115-2128.
51. J. Wang, X. Yuanzhi, Y. Zhi, H. Renhuan, C. Jing, W. Raorao and Y. Lin, *Current Drug Metabolism*, 2013, **14**, 891-899.
52. P. R. Kennedy, *Journal of Neuroscience Methods*, 1989, **29**, 181-193.
53. W. He, C. R. Halberstadt and K. E. Gonsalves, *Biomaterials*, 2004, **25**, 2055-2063.
54. J. C. Chang, G. J. Brewer and B. C. Wheeler, *Biomaterials*, 2003, **24**, 2863-2870.

55. C. D. James, A. J. H. Spence, N. M. Dowell-Mesfin, R. J. Hussain, K. L. Smith, H. G. Craighead, M. S. Isaacson, W. Shain and J. N. Turner, *Ieee Transactions on Biomedical Engineering*, 2004, **51**, 1640-1648.
56. E. M. Regan, A. Taylor, J. B. Uney, A. D. Dick, P. W. May and J. McGeehan, *Ieee Journal on Emerging and Selected Topics in Circuits and Systems*, 2011, **1**, 557-565.
57. A. P. Hopper, J. M. Dugan, A. A. Gill, E. M. Regan, J. W. Haycock, S. Kelly, P. W. May and F. Claeysens, *Materials Science & Engineering C-Materials for Biological Applications*, 2016, **58**, 1199-1206.
58. P. W. May, E. M. Regan, A. Taylor, J. Uney, A. D. Dick and J. McGeehan, *Diamond and Related Materials*, 2012, **23**, 100-104.
59. Y. Cai, F. Edin, Z. Jin, A. Alexsson, O. Gudjonsson, W. Liu, H. Rask-Andersen, M. Karlsson and H. Li, *Acta Biomaterialia*, 2015.
60. E. Kaivosoja, P. Suvanto, G. Barreto, S. Aura, A. Soininen, S. Franssila and Y. T. Konttinen, *Journal of Biomedical Materials Research Part A*, 2013, **101**, 842-852.
61. L. R. Hochberg, D. Bacher, B. Jarosiewicz, N. Y. Masse, J. D. Simeral, J. Vogel, S. Haddadin, J. Liu, S. S. Cash, P. van der Smagt and J. P. Donoghue, *Nature*, 2012, **485**, 372-U121.
62. D. Bacher, B. Jarosiewicz, N. Y. Masse, S. D. Stavisky, J. D. Simeral, K. Newell, E. M. Oakley, S. S. Cash, G. Friehs and L. R. Hochberg, *Neurorehabilitation and Neural Repair*, 2015, **29**, 462-471.
63. E. Zrenner, K. U. Bartz-Schmidt, H. Benav, D. Besch, A. Bruckmann, V.-P. Gabel, F. Gekeler, U. Greppmaier, A. Harscher, S. Kibbel, J. Koch, A. Kusnyerik, T. Peters, K. Stingl, H. Sachs, A. Stett, P. Szurman, B. Wilhelm and R. Wilke, *Proceedings of the Royal Society B-Biological Sciences*, 2011, **278**, 1489-1497.
64. L. Greenemeier, FDA Approves First Retinal Implant, <http://www.nature.com/news/fda-approves-first-retinal-implant-1.12439>, (accessed November, 2015).
65. J. D. Weiland, W. T. Liu and M. S. Humayun, *Annual Review of Biomedical Engineering*, 2005, **7**, 361-401.
66. K. Ganesan, D. J. Garrett, A. Ahnood, M. N. Shivdasani, W. Tong, A. M. Turnley, K. Fox, H. Meffin and S. Praver, *Biomaterials*, 2014, **35**, 908-915.
67. A. Bendali, L. Rousseau, G. Lissorgues, E. Scorsoni, M. Djilas, J. Degardin, E. Dubus, S. Fouquet, R. Benosman, P. Bergonzo, J.-A. Sahel and S. Picaud, *Biomaterials*, 2015, **67**, 73-83.
68. P. P. Sheng and T. H. Etsell, *Waste Management & Research*, 2007, **25**, 380-383.
69. J. J. Gracio, Q. H. Fan and J. C. Madaleno, *J. Phys. D: Appl. Phys.*, 2010, **43**, 1-22.
70. M. L. Hartsell and L. S. Plano, *Journal of Materials Research*, 1994, **9**, 921-926.
71. M. Nagase, K. Watanabe, H. Umezawa and S. Shikata, *Japanese Journal of Applied Physics*, 2012, **51**.
72. C. K. Gupta, *Extractive Metallurgy of Molybdenum*, CRC Press, United States of America, 1992.